

Yet Another Hydrodynamic Model with Correlated Parameters for Silicon Devices

Muhammad H. El-Saba

Ain-Shams University, Faculty of Engineering, Dept of Electronic Engineering, Cairo, Egypt

Abstract In this paper we present a complete hydrodynamic model (HDM) describing the transport of charge carriers in semiconductor devices with arbitrary band structure. The model is appended with advanced physical models for almost all the physical parameters of interest in modern Si Devices. These parameters are inter-related via the carrier energy relaxation time. An improved analytical model of the carrier heat flux, on the basis of a fourth moment of the Boltzmann transport equation (BTE), is also presented. In order to resolve the heat evacuation problems in SOI and power devices, the model is coupled with a lattice heat conservation equation. The transport of hot carriers is simulated, according to the proposed HDM and the results are compared with the conventional data obtained using the drift-diffusion model (DDM) and MC simulation. We show from the HD simulation, the effect of the energy relaxation time value on the hot carrier transport in general and the breakdown voltage in particular, of both MOSFETs and bipolar devices.

Keywords Semiconductor Devices, Hydrodynamic Modelling, Simulation, Semiclassical Transport Theory, Impact Ionization, Injection, Hot Carriers

1. Introduction

For a gas of charge carriers of q -type, where q stands for (n) for electrons or (p) for holes, the semiclassical Boltzmann transport equation (BTE) may be written as follows, when charge carriers are not strongly correlated[1]

$$\partial f_q / \partial t + u_q \cdot \nabla f_q - (\mathbf{F} / \hbar) \cdot \nabla_k f_q = (\partial f_q / \partial t)_{col} \quad (1.a)$$

where $f_q = f_q(\mathbf{k}, \mathbf{x}, t)$ is the carrier distribution function of the q -type gas in the phase space, u_q is the group velocity of carriers, $\mathbf{F} = \pm e(\boldsymbol{\zeta} + u_q \times \mathbf{B})$ is the applied force due to electric field $\boldsymbol{\zeta}$ and magnetic field \mathbf{B} and $(\partial f_q / \partial t)_{col}$ is the rate of change of the distribution function due to the internal collisions between the charge carriers and the crystal lattice (phonons and other defects).

Since the validity of the semiclassical transport approaches for simulating extremely scaled devices (sub 0.1 μm) and ultra fast devices (working up to the terahertz range) has been lately a subject of debate, we just remind here the main assumptions on which the BTE in semiconductors is based[2].

- Collisions are localized in space, so that the mean free path of charge carriers is much greater than the de-Broglie wavelength,

- Collisions are instantaneous in time such that the collision time is much smaller than the time between

subsequent collisions,

- External electric field force does not vary greatly over small distances in the order of wave packet length,

- Particles are weakly correlated (Bogoliubov assumption[3]) and the many body effect is negligible.

Mathematically speaking, the BTE is valid as long as the following Barker condition is realized[4]:

$$\left| \frac{e \zeta_m \hbar q \tau_c}{2 m^*} \right| \leq \frac{2 \hbar}{\tau_{cc}} \quad (1.b)$$

where ζ_m is the maximum applied electric field, m^* is the carrier effective mass, τ_{cc} is collision time and τ_c is mean free time between collisions and $q = k - k'$ is the wave vector of (emitted or absorbed) phonons during collisions.

For strongly ionized gasses and degenerate semiconductors, where particle-particle collisions are not negligible, the Boltzmann transport equation may be replaced by the Fokker-Planck equation[5-6]. For ultra small devices, whose active layers dimensions (at least one of them) are in the order of De Broglie wavelength, the BTE should be replaced by one of the quantum transport formulations[7-11], like the Wigner-Boltzmann transport equation (WBTE) [9-11]. However, there exist several approaches to include the degeneracy effects and quantum corrections to the semiclassical transport models (e.g., [12-13]).

The solution of semiclassical BTE is carried out by a variety of methods[14-26], among which the iterative methods[15], the matrix methods[16], the Monte Carlo method[17-21], the cellular automata method[22], truncated expansion (usually in Legendre polynomials and spherical

* Corresponding author:

mhs1308@hotmail.com (Muhammad H. El-Saba)

Published online at <http://journal.sapub.org/msse>

Copyright © 2012 Scientific & Academic Publishing. All Rights Reserved

harmonics) methods[23-26]. In addition, the so-called energy transport model (ETM) and moment methods[27], which are sometimes called the hydrodynamic model (HDM), have been also used to solve the BTE in the hot carrier regime. In the ETM approach the distribution function is decomposed into an even and odd parts and the collision term is expressed using a microscopic relaxation time approximation[28].

The hydrodynamic description of the gas of charge carrier in semiconductors consists in the study of the evolution of certain macroscopic quantities, whose physical meaning is significant and whose quantity is eventually measurable. So, the HDM is constructed by multiplying the semiclassical BTE with a number of *weight functions* and integrating these equations over the phase or momentum space, so that a set of differential equations in physical space and time is obtained. This method is hence an averaging process that leads to the loss of some microscopic information in the distribution function. However, in many practical cases the resultant average (or macroscopic) parameters retained by the equations in the physical space are sufficient to capture the essential features of the carrier transport phenomena. The HDM has been widely used in the study of aerodynamic flow, and was suggested to study the hot electron transport in multivalley semiconductor devices by Bløtejaer[29]. Since then, several contributions have been introduced to improve the hot carrier transport models in semiconductors and the HDM in particular[30-47]. For instance, the nonparabolicity of energy bands has been included in the HDM for the first time by Thoma et al[38]. The energy transport model ETM was reformulated by Chen, Kan and Ravaoli, who assumed non-Maxwellian and nonparabolicity correction factors, to solve the contradiction involved in evaluating a non-zero heat flux term for a Maxwellian distribution[39]. Also, the number of considered moments in the HDM has been increased in order to improve the HDM accuracy[44]. Unfortunately, all the added improvements to the HDM were associated with the addition of a huge number of new physical parameters[45-46]. On the other hand, some authors neglected the role of some important parameters in order to reduce the complexity of the model. This led to several paradoxal results and the failure of the HDM, in certain situations[47]. We try here to generalize the previously introduced models while reducing the number of physical parameters, by correlating them all to the energy relaxation time. We start by introducing the system of hydrodynamic equations in section II. In section III we discuss the system closure hypotheses. We present the physical definition of the carrier temperature. In section IV we present an almost complete description of the physical parameters in the bulk of semiconductor devices. Finally we present our conclusions in section VIII.

2. System of Hydrodynamic Equations

The multiplying weight functions in the HDM for semiconductors are usually chosen as powers of increasing

order of the carrier vector \mathbf{k}_q , or carrier group velocity \mathbf{u}_q , or even the carrier momentum \mathbf{p}_q . The powers of these parameters are usually formatted using some appropriate scaling factors to get physically meaningful quantities. For instance, if we adopt the powers of the carrier group velocity as weight functions (e.g., 1 , \mathbf{u}_q and u_q^2), then we use the carrier energy $E_q = \frac{1}{2}m_q^*u_q^2$, instead of u_q^2 as the second-order multiplier. So, the set of conservation equations of carrier concentration, momentum and energy may be obtained by multiplying the BTE by the first powers of the carrier group velocity \mathbf{u}_q (e.g., 1 , \mathbf{u}_q and E_q), and then integrating the two sides of the resulting equations over the whole \mathbf{k} -space (see Appendix I). For the sake of simplicity and brevity we write here only the electron equations in a single-valley semiconductor. In multi-valley semiconductors, we may assume a single lumped valley or write similar equations for each valley of the semiconductor[37]. The electron density-, momentum- and energy- conservation equations, in a semiconductor, can be put in the following form:

$$\partial n / \partial t + \nabla \cdot (n \mathbf{v}_n) = [\partial n / \partial t]_{\text{col}} \quad (2.a)$$

$$\partial (n \mathbf{v}_n) / \partial t + \nabla \cdot (m_n^{-1} \mathbf{P}_n) + \nabla \cdot (n \mathbf{v}_n \otimes \mathbf{v}_n) = n m_n^{-1} \cdot \mathbf{F} + [\partial (n \mathbf{v}_n) / \partial t]_{\text{col}} \quad (2.b)$$

$$\partial (n \omega_n) / \partial t + \nabla \cdot \mathbf{S}_n = n \mathbf{v}_n \cdot \mathbf{F} + [\partial (n \omega_n) / \partial t]_{\text{col}} \quad (2.c)$$

where n , \mathbf{v}_n , \mathbf{P}_n and ω_n are the electron concentration, mean velocity, electrokinetic pressure tensor and mean energy, respectively. Also, \mathbf{S}_n is the electron energy flow and m_n^{-1} is the mean inverse mass of electrons. We dully note that we don't adopt the effective mass approximation here, and the second derivative of electron energy just appears as a result of the averaging process in the \mathbf{k} -space (Appendix I). Therefore, the mean inverse mass of carriers is generally a tensor whose components $m_n^{-1}{}_{(ij)} = (1/\hbar^2) \langle \partial^2 E_n / \partial k_i \partial k_j \rangle$ are supposed functions of the mean carrier energy. When the energy band structure of the semiconductor material is assumed parabolic, m_n^{-1} is a constant and equal to the conventional electron inverse effective masse (m_n^*)⁻¹ at the bottom of conduction band. However, in this work we consider m_n as a scalar quantity averaged over the semiconductor valleys $m_n^{-1} = \frac{1}{3} \sum m_n^{-1}{}_{(ij)}$. At the bottom of conduction band the average mass will be denoted by m_{no} and its value in Si, according to optical measurements is about $0.275 m_o$. The subscript 'col.' in the above equations means the rate of change of the quantity between brackets due to electron gas collisions with the semiconductor crystal lattice and its defects. The sign \otimes stands for the tensorial product of two terms such that:

$$\nabla \cdot (n \mathbf{v}_n \otimes \mathbf{v}_n) = \mathbf{v}_n \nabla \cdot (n \mathbf{v}_n) + (n \mathbf{v}_n \cdot \nabla) \mathbf{v}_n \quad (3.a)$$

The electrokinetic pressure tensor in the above equations is defined as follows:

$$\mathbf{P}_n \equiv n m_n \langle (\mathbf{u}_n - \mathbf{v}_n) \otimes (\mathbf{u}_n - \mathbf{v}_n) \rangle \quad (3.b)$$

We discuss the significance of this definition in the following section. The carrier energy flow (or energy flux) is given by the following expression, for electrons:

$$\mathbf{S}_n = n \langle E_n \mathbf{u}_n \rangle = \mathbf{Q}_n + (n \omega_n + \mathbf{P}_n) \cdot \mathbf{v}_n \quad (4.a)$$

where \mathbf{Q}_n is called the electron heat flux. In the effective mass approximation, where we express the electron energy by $E_n = \frac{1}{2} m_n^* u_n^2$, the electron heat flux vector \mathbf{Q}_n is defined as the third central moment of the electron distribution function f_n :

$$\mathbf{Q}_n = n \langle \frac{1}{2} m_n^* (\mathbf{u}_n - \mathbf{v}_n) \cdot (\mathbf{u}_n - \mathbf{v}_n)^2 \rangle = \frac{1}{2} \int m_n^* |\mathbf{u}_n - \mathbf{v}_n|^2 (\mathbf{u}_n - \mathbf{v}_n) \cdot f_n(\mathbf{x}, \mathbf{k}, t) d^3 \mathbf{k} \quad (4.b)$$

So, the heat flux component $\mathbf{Q}_{n(i)}$ is the flux of random thermal energy across a surface with its normal oriented in the i^{th} direction. However, as the electron distribution function is not known we don't make use of this equation in our model. We fully note that the formal definition of the gas pressure tensor $\mathbf{P}_{n(ij)}$ is the flux of the i^{th} component of the momentum across a surface element moving with the mean velocity oriented with its normal in the j^{th} direction[48], such that:

$$\mathbf{P}_{n(ij)} \equiv \langle \rho_{n(ij)} (\mathbf{u}_{ni} - \mathbf{v}_{ni})(\mathbf{u}_{nj} - \mathbf{v}_{nj}) \rangle \quad (5.a)$$

where $\rho_{n(ij)}$ is the mass density of the gas. In the ideal gas theory, the gas mass density is a macroscopic quantity and ρ_n is taken outside the averaging brackets. So, the gas mass density is given by:

$$\rho_{n(ij)} = n m_{n(ij)}, \text{ with } m_{n(ij)}^{-1} = (1/\hbar^2) \int [\partial^2 E_n / \partial k_i \partial k_j] f_n(\mathbf{x}, \mathbf{k}, t) d^3 \mathbf{k} / \int f_n(\mathbf{x}, \mathbf{k}, t) d^3 \mathbf{k} \quad (5.b)$$

such that $\mathbf{P}_n \equiv \mathbf{P}_n$. However, in classical transport models, the electron gas mass density is usually related to the electron effective mass such that $\rho_n = n m_n^*$. Hence, our definition of the gas pressure, \mathbf{P}_n , is different from the classic definition of electron gas pressure tensor, \mathbf{P}_n :

$$\mathbf{P}_n = n \langle m_n^* (\mathbf{u}_n - \mathbf{v}_n) \otimes (\mathbf{u}_n - \mathbf{v}_n) \rangle \quad (5.c)$$

Therefore, the electrokinetic pressure tensor \mathbf{P}_n may be related to the classic definition \mathbf{P}_n via a correction factor, g_n , such that:

$$\mathbf{g}_n = \mathbf{P}_n \cdot \mathbf{P}_n^{-1} = [m_n^* (\mathbf{u}_n - \mathbf{v}_n) \otimes (\mathbf{u}_n - \mathbf{v}_n)] \cdot [m_n \langle (\mathbf{u}_n - \mathbf{v}_n) \otimes (\mathbf{u}_n - \mathbf{v}_n) \rangle]^{-1} \quad (5.d)$$

We call this factor, the electron gas pressure g -factor. This factor can be calculated from MC simulation in the bulk of semiconductor with arbitrary band structure.

In absence of magnetic field, the applied force on electrons is given by $\mathbf{F} = -e\boldsymbol{\zeta}$, where the electric field $\boldsymbol{\zeta}$ is equal to the negative gradient of the electrostatic potential ψ . In heterogeneous devices, the applied force on electrons is given by $\mathbf{F} = -\nabla E_c$, where $E_c = (E_{co} - e\psi)$ and E_{co} is the edge of the conduction band. Similarly, the applied force on holes is $\mathbf{F} = \nabla E_v$, where $E_v = (E_{vo} + e\psi)$ and E_{vo} being the edge of the valence band. The electrostatic potential distribution can be found by solving the Poisson equation:

$$\nabla \cdot (-\epsilon \nabla \psi + \mathbf{P}) = e(p - n + \text{Dop} + N_t) \quad (6)$$

where p is the hole concentration, ϵ is the dielectric constant, \mathbf{P} is the polarization vector, N_t is the density of traps and $\text{Dop} = |N_d^+ - N_a^-|$ is the net ionized concentration in the semiconductor.

3. Closing the System of Hydrodynamic Equations

In order to close the system of conservation equations for charge carrier density, average momentum and average energy (2-a,b,c) we usually adopt some assumptions to approximate the terms which depend on the knowledge of the distribution function. The main assumptions are usually concerned with the following items:

1. definition of the carrier gas pressure and temperature,
2. approximation of collision terms,
3. modeling the heat flux term (the third center moment of the distribution function), and
4. modeling any other higher moment terms, if the number of moments is greater than 3.

When the kinetic pressure of the gas of electrons is considered as a scalar quantity, one can define the electron gas temperature, T_n , by the law of perfect gases $\mathbf{P}_n = n k_B \mathbf{T}_n$. This assumption does not imply a spherically-symmetric distribution function about its mean value in the momentum space (like the displaced Maxwellian distribution). Equation (5-a) can be merged with the hypothesis of the perfect gas law, in one relation defining the electron gas temperature as follows:

$$k_B \mathbf{T}_n = \langle m_n^* (\mathbf{u}_n - \mathbf{v}_n) \otimes (\mathbf{u}_n - \mathbf{v}_n) \rangle \quad (7)$$

This coincides with the physical definition of the temperature as a measure of the average kinetic energy of the gas particles[49]. Using the above definitions of the electron gas pressure and temperature, we can easily prove that the mean electron energy ω_n is related to the scalar electron temperature T_n and scalar average mass m_n as follows:

$$\omega_n = \langle E_n \rangle = \langle \frac{1}{2} m_n^* u_n^2 \rangle = \frac{1}{2} g_n m_n v_n^2 + 3/2 k_B T_n \quad (8)$$

Although we make use of the expression $E_n = \frac{1}{2} m_n^* u_n^2$ in order to derive the above relation between ω_n and T_n , the eventual error due to the effective mass approximation is absorbed in the gas pressure correction factor, which can be calculated by MC simulation. However, it is well known that the convection part of the the average electron energy is generally small compared the thermal part, except for device regions where the velocity overshoot is pronounced.

As for the collision terms, we make use of the macroscopic relaxation time approximation[31]. In this approximation, the collision term in the momentum conservation equation is expressed in terms of a macroscopic momentum relaxation time τ_{mn} , as follows:

$$[\partial n \mathbf{v}_n / \partial t]_{\text{col.}} = -n \mathbf{v}_n / \tau_{mn} + \mathbf{v}_n [\partial n / \partial t]_{\text{col.}} \quad (9.a)$$

Also, the collision term in the energy conservation equation can be expressed in terms of a macroscopic energy relaxation time τ_{wn} , as follows:

$$[\partial n \omega_n / \partial t]_{\text{col.}} = -n (\omega_n - \omega_0) / \tau_{wn} + \omega_n [\partial n / \partial t]_{\text{col.}} \quad (9.b)$$

where $\omega_0 = 3/2 k_B T_L$ is the electron energy at thermal equilibrium and T_L is the lattice temperature. Note that the collision term in the above two equations is decomposed into two terms. So, the momentum and energy relaxation times, include the effect of collisions over optical while the effect of impact ionization collisions is included in the $[\partial n / \partial t]_{\text{col.}}$. The collision term $[\partial n / \partial t]_{\text{col.}}$, which appears explicitly in the carrier density conservation equation can be expressed as follows:

$$[\partial n / \partial t]_{\text{col}} = - (n - n_0) / \tau_n = - U \quad (9.c)$$

where ($U = R - G$) is the net recombination-generation rate in the semiconductor. Note that the recombination rate, R , regroups the relevant recombination mechanisms in the semiconductor device (e.g., radiative, Shockley-Reed-Hall and Auger recombination mechanisms[50]). Also, the generation rate, G , regroups the applicable generation mechanisms in the semiconductor device (e.g., thermal and optical generation as well as the generation by impact ionization mechanism).

Using the relaxation-time approximation and our definition of the carrier temperature, the set of hydrodynamic equations (HDE's) can be formulated as follows for a single valley semiconductor:

$$e \partial n / \partial t - \nabla \cdot \mathbf{J}_n = e(G - R) \quad (10.a)$$

$$\mathbf{J}_n - n \mu_n m_n d[\mathbf{v}_n] / dt = e n \mu_n \zeta + k_B \mu_n m_n \nabla \cdot (n \mathbf{g}_n m_n^{-1} \cdot \mathbf{T}_n) \quad (10.b)$$

$$\partial(n \omega_n) / \partial t + \nabla \cdot \mathbf{S}_n = \zeta \mathbf{J}_n + \omega_n (G - R) - n(\omega_n - \omega_0) / \tau_{wn} \quad (10.c)$$

The electron drift mobility μ_n is defined as follows:

$$\mu_n = e \tau_{nn} m_n^{-1} \quad (11.a)$$

Similar equations can be written for holes. We dully note that the average electron energy ω_n is measured *above* the conduction band edge E_c , while the average hole energy ω_p is measured *under* the valence band edge E_v .

In steady state (up to the terahertz frequency range), the carrier momentum conservation equations can be further simplified by suppressing the partial time-derivatives so that:

$$\begin{aligned} & \mathbf{J}_n - n \mu_n m_n (\mathbf{v}_n \cdot \nabla)(\mathbf{v}_n) \\ & = e n \mu_n \zeta + k_B \mu_n m_n \nabla \cdot (n \mathbf{g}_n m_n^{-1} \cdot \mathbf{T}_n) \end{aligned} \quad (11.b)$$

$$\begin{aligned} & \mathbf{J}_p + p \mu_p m_p (\mathbf{v}_p \cdot \nabla)(\mathbf{v}_p) \\ & = e p \mu_p \zeta - k_B \mu_p m_p \nabla \cdot (p \mathbf{g}_p m_p^{-1} \cdot \mathbf{T}_p) \end{aligned} \quad (11.c)$$

The above conservation equations are similar to the current equations of the isothermal DDM, except for the acceleration and thermal diffusion terms. Also the carrier energy flow (or energy flux) can be put in the following forms, for electrons and holes:

$$\mathbf{S}_n = \mathbf{Q}_n - (\omega_n + \mathbf{g}_n k_B \mathbf{T}_n) \cdot (\mathbf{J}_n / e) \quad (11.d)$$

$$\mathbf{S}_p = \mathbf{Q}_p + (\omega_p + \mathbf{g}_p k_B \mathbf{T}_p) \cdot (\mathbf{J}_p / e) \quad (11.e)$$

As indicated by (4-b), the carrier heat flux terms is defined in terms of the carrier distribution function, which is unknown. Therefore, the carrier-heat flux is usually modeled by the Fourier relation[51]:

$$\mathbf{Q}_n = - k_n \nabla T_n \quad (12.a)$$

where k_n is the electron thermal conductivity. The carrier thermal conductivity is usually modeled by the Wiedemann - Franz law, which states:

$$k_n = \gamma_n (k_B / e)^2 T_n \sigma_n \quad (12.b)$$

where σ_n is the electrical conductivity and γ_n is the Lorenz number (for electrons). In the original Wiedeman-Franz formulation (using the microscopic relaxation time approximation) γ_n is given by:

$$\gamma_n = 5/2 + r \quad (12.c)$$

where r is an exponent in the microscopic relaxation time τ_{Dn} expression, which is given by:

$$\tau_{Dn} = \tau_0 (k_B T_L / E_n)^r \quad (12.d)$$

A more rigorous approach for modelling the carrier heat flux term consists in taking the third moment of the BTE into account. This procedure increases the number of differential equations to be solved and the number of parameters of the HDM. However, we show in section 5.4 how to derive a more accurate model of the carrier heat flux term and the Lorentz number, on the basis of the third moment of the BTE. We do this without increasing the number of differential equations of the HDM.

4. About the Definition of the Carrier Temperature

In this section we compare the different approaches for modeling the carrier temperature. Formally, temperature is a property which governs the transfer of thermal energy, or heat, between one system and another. The electronic temperature concept was initially introduced in 1947 by Fröhlich[52], and since then it has been exploited by several authors to model the high-field transport in semiconductors. In the isothermal drift-diffusion model (DDM), the carriers temperature is assumed equal to the lattice temperature T_L . However, the so-called static electron temperature T_n may be roughly estimated from the electric field distribution in several ways[53]. For instance, the static temperature may be defined as follows:

$$T_n (\text{static}) = T_L (\mu_{n0} / \mu_n(\zeta)) = T_L [1 + (\mu_{n0} \zeta^{//} / v_n^{sat})^2]^{1/2} \quad (13)$$

where μ_n is the electron drift mobility, v_n^{sat} is the electron saturation velocity and μ_{n0} is the low-field drift mobility. Also, $\zeta^{//}$ is the parallel component of the electric field to the electron current density such that $\zeta^{//} = \zeta \cdot \mathbf{J}_n / |\mathbf{J}_n|$. The above equation is based on the assumption that the parallel component of the diffusion coefficient is almost constant and independt of the electric field[33]. Such static forms of the carrier temperature exclude the lag effect between the electric field and the carrier temperature, and hence the velocity overshoot phenomenon will not be observed. However, the definition of the carrier temperature in the Monte Carlo simulation is given by:

$$3/2 k_B T_n = \langle E_n(k) \rangle \quad (14.a)$$

Also, the carrier temperature in the conventional hydrodynamic models, where the effective mass approximation is assumed and the anisotropy of the distribution function is ignored, is defined by:

$$3/2 k_B T_n = 1/2 m_n^* \langle |\mathbf{u}_n - \mathbf{v}_n|^2 \rangle \quad (14.b)$$

It is well known, that the above two definitions result in different temperatures[38]. In fact, the conventional hydrodynamic definition (14-b) is implicitly based on the displaced Maxwellian distribution at the electronic temperature.

$$f_m(k) = A \cdot [n / (k_B T_n)]^{3/2} \cdot \exp(-1/2 m_n^* (\mathbf{u}_n(k) - \mathbf{v}_n)^2 / k_B T_n) \quad (15.a)$$

where A is a constant. Assuming that the collisions are fully randomized, such that the drift energy may be neglected with respect to the thermal energy, then the electron distribution may be approximated to the so-called heated Maxwellian as follows:

$$f_m(E_n) = B \cdot [n / (k_B T_n)]^{3/2} \cdot \exp(-E_n / k_B T_n) \quad (15.b)$$

where $E_n = \frac{1}{2} m_n^* \mathbf{u}_n^2$ is the electron energy and B is constant. According to Staratton[28], the electronic temperature has no physical meaning, unless the distribution function is a displaced Maxwellian as described by equation (15). However, the Maxwellian distribution is only valid near equilibrium, and in highly doped regions, where carrier-carrier collisions are dominant. In fact, it has been confirmed by several authors (e.g., [21]) that the energy distribution function is not Maxwellian at high electron energies. In the so-called improved energy transport model[39], the nonparabolicity of the band structure is taken into account and the distribution function $f_m(E)$ is appended by a non-Maxwellian factor γ , such that:

$$f_m(E_n) = (1 + \gamma \cdot E_n / k_B T_n) \cdot f_m(E_n) \quad (16.a)$$

with $f_m(E)$ is the heated Maxwellian distribution function at an elevated temperature T_n . Then, a modified (or equivalent) carrier temperature T_m is defined as follows:

$$T_m = T_n (1 + \gamma) \quad (16.b)$$

However, referring to our system of HDE's (8), we make use of the formal definition for the electron temperature tensor:

$$k_B \mathbf{T}_n = \langle m_n^* (\mathbf{u}_n - \mathbf{v}_n) \otimes (\mathbf{u}_n - \mathbf{v}_n) \rangle \quad (17.a)$$

When the carrier temperature tensor is reduced to a scalar quantity (such that $\mathbf{T}_n = T_n \mathbf{I}$ where \mathbf{I} is the unity tensor), then the above definition may be simply written as follows:

$$3/2 k_B T_n = \frac{1}{2} g_n m_n \langle |\mathbf{u}_n - \mathbf{v}_n|^2 \rangle \quad (17.b)$$

In this case the g-factor may be calculated from the following relation:

$$g_n = \mathbf{P}_n \cdot \mathbf{P}_n^{-1} = \langle m_n^* |\mathbf{u}_n - \mathbf{v}_n|^2 \rangle / m_n \langle |\mathbf{u}_n - \mathbf{v}_n|^2 \rangle \quad (17.c)$$

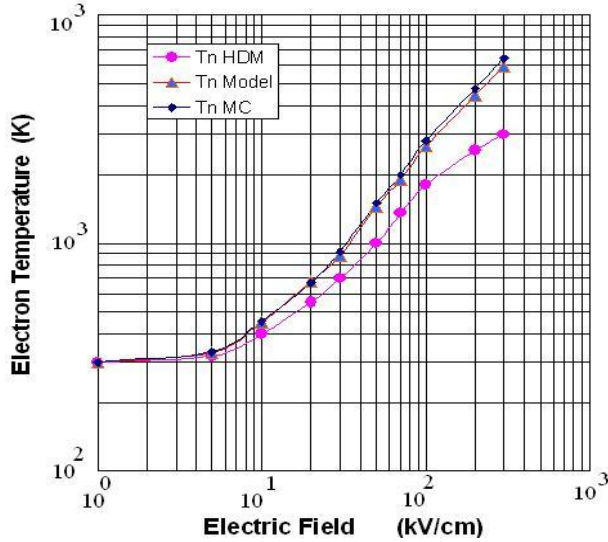


Figure 1. Electron temperature according to MC[29], classic HDM and our model

Figure 1 depicts the variation of T_n according to MC (with a nonparabolicity factor 0.5 eV^{-1}) and the classic hydrodynamic model (14-b) and to our definition (17-b). Note that assuming $g_n \approx 1$ brings an error less than 3% in T_n , for electric fields up to 300 kV/cm. This error is less drastic than the error encountered when neglecting the convective part in the calculation of the electron energy. In fact, most of

the commercial simulators neglect totally the convection part of the carrier mean energy. If we adopt the assumption of unity g_n , we can drop the g_n factor from the above system of hydrodynamic equations while keeping the non-parabolicity effects, via the average mass term. In this case, the scalar temperature definition reduces to:

$$3/2 k_B T_n \approx \frac{1}{2} m_n \langle |\mathbf{u}_n - \mathbf{v}_n|^2 \rangle \quad (17.d)$$

This approximation means that we assume the electrokinetic pressure tensor $\mathbf{P}_n = nk_B \mathbf{T}_n$, and may be considered as a closure condition for the set of HDEs. However, if later full-band MC (FBMC) showed a significant deviation of the g-factor from unity at very high fields, it could be easily retained in the proposed HDM to get more accurate results.

5. Energy-Dependent Physical Parameters

The accurate modelling of transport parameters, as the carrier drift mobility and impact ionization rate at high energies, is vital in any transport model. In the DDM, these parameters were usually expressed as functions of the local electric field [54-55]. Nevertheless, we know that these parameters express physical mechanisms involving energy exchange and should be expressed as functions of the carrier energy, rather than the local electric field. Fortunately, the solution of the HDM produces such information about the carrier energy distribution and permits to express these parameters in a physical manner, along the semiconductor device. In the following subsections, we discuss the modelling of the energy-dependent physical parameters in the bulk of silicon devices.

5.1. Carrier Drift Mobility

5.1.1. Carrier Drift Mobility in the Bulk

In the drift-diffusion model, the high-field drift mobility in the bulk of a semiconductor is usually expressed by the Caughey-Thomas model, in its scaled form [56]:

$$\mu_{no}(\zeta) = \frac{\mu_{no}}{\left[1 + \left(\frac{\mu_{no} \zeta}{v_n^{sat}} \right)^2 \right]^{1/2}} \quad (18.a)$$

where $\mu_{no} = \mu_{no}(DOP, T_L, n, p)$ is the low-field mobility of electrons, which is related to doping, temperature and injection level, and may be expressed by a suitable model, e.g., Dorkel-Leturcq[57] or Klassen[58] models. Also v_n^{sat} is the electron saturation velocity and may be expressed by the model of Canali et al. [59]:

$$v_n^{sat} = 2.4 \times 10^7 / [1 + 0.8 \exp(T_L / 600)] \text{ cm/s} \quad (18.b)$$

However, in the hydrodynamic model where the carrier average energy can be determined, the high-field mobility can be expressed in terms of the carrier mean energy $\omega_{n,p}$. The energy-dependent drift mobility relation may be written in the following form [60]:

$$\mu_n^{-1} = \mu_{no}^{-1} \left[1 + \frac{\mu_{no}}{e [v_n^{sat}]^2} \left(\frac{\omega_n - \omega_o}{\tau_{on}} \right) \right] \quad (18.c)$$

This model resembles the model of **Hänsch** and **Mattausch**[61], but we consider an energy-dependent relaxation time and we make no a priori assumption about the distribution function in its derivation[62]. Figure 2(a) shows the variation of electron drift mobility as a function of electron temperature, according to our model and according to the model of Hänsch-Mattausch. In our model τ_{on} is taken from MC simulation, as shown in Figure 4(a). In order to compare our model with the field-dependent phenomenological relations, one can substitute equation (18-b) into the set of HDE's in steady state homogeneous case to obtain:

$$(\mu_{no}/\mu_n) = (\mu_n/\mu_{no}) (\mu_{no} \zeta / v_n^{sat})^2 + 1 \quad (19.a)$$

The solution of this quadratic equation (in μ_n) is given by the following relation:

$$\mu_n(\zeta_{//}) = \frac{2\mu_{no}}{1 + \sqrt{1 + [2\mu_{no}\zeta_{//} / v_n^{sat}]^2}} \quad (19.b)$$

where we replaced ζ by the parallel field component $\zeta_{//}$, which is responsible of carrier heating, to satisfy the Thorber scaling theory[63]. As shown in Figure 2(b), this model coincides with the conventional field-dependent Caughey-Thomas mobility model[56] as well as the measured drift mobility, according to Canali et al[59]. The change of saturation velocity with lattice temperature may be also modelled as follows:

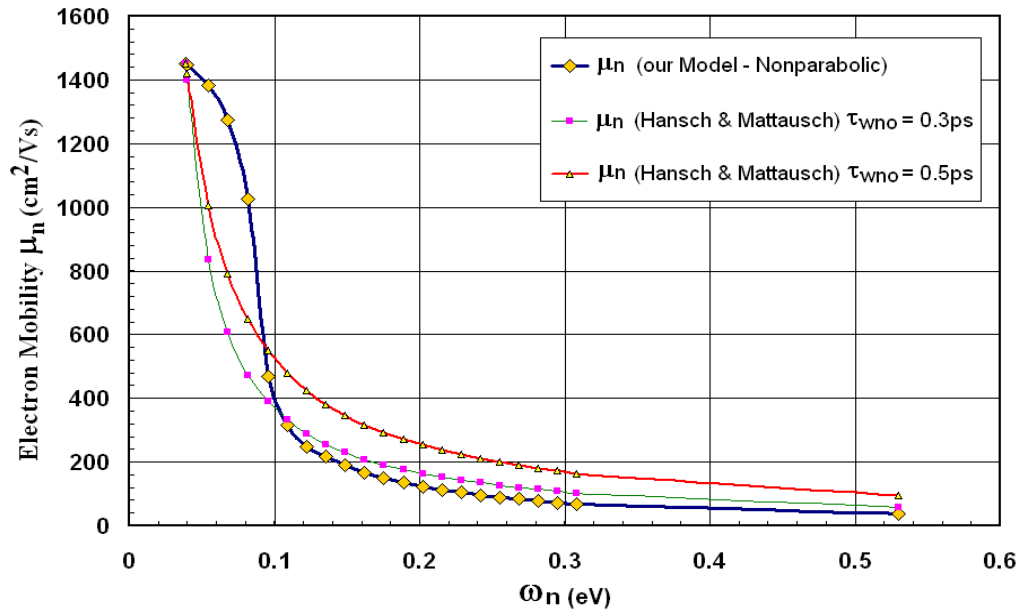


Figure 2(a). Electron drift mobility in Si at 300K versus electron temperature, according to the model of Hänsch-Mattausch with different values of τ_{ono} [43] and according to our model

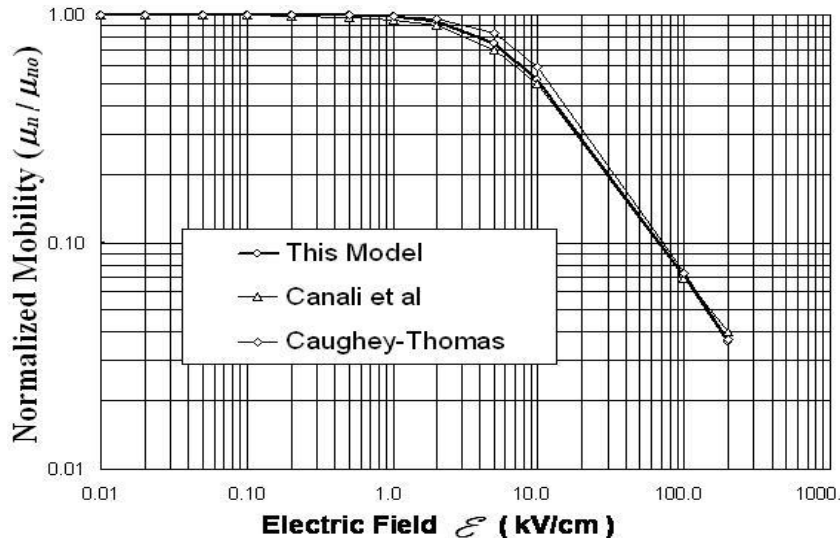


Figure 2(b). Electron drift mobility in Si at 300K, according to Canali et al[56], Caughey-Thomas model[52] and our model

5.1.2. Carrier Drift Mobility near the Surface

The drift mobility near the surface of a semiconductor is greatly reduced because of the additional scattering mechanisms due to the rupture of crystal periodicity, the surface phonons, the surface roughness and the eventual presence interface states. In addition, the presence of confined electrons into a thin layer near the surface of MOSFETs (the inversion layer) gives rise to quantization effects (subbands). As suggested by Sabins and Clemens[64], the reduction in the *effective* surface mobility may be expressed as a unique function of the effective vertical field ζ_{\perp} . The most famous model of the surface mobility in MOSFET devices has been, for long time, the Yamaguchi model[65]:

$$\mu_c(\zeta_{\perp}) = \frac{\mu_b}{1 + \sqrt{1 + (\zeta_{\perp} / \zeta_c)^2}} \quad (20)$$

where $\zeta_{\perp} = |\zeta_x J_n| / |J_n|$, ζ_c is a constant (1.49×10^4 V/cm for electrons and 1.87×10^4 V/cm for holes in Si), and $\mu_b = \mu_n(Dop, T_L, n, p, \zeta_{//})$ is the bulk drift mobility. According to Hänsch-Mattausch model[61], the drift mobility along the semiconductor surface is given by the following relation:

$$\mu_c = \frac{2\mu_s}{1 + \sqrt{1 + [2\mu_s \zeta_{//} / v_n^{sat}]^2}} \quad (21.a)$$

which resembles equation (19-b) but with the low-field mobility μ_{n0} replaced with the reduced surface mobility μ_s , which is given by:

$$\mu_s(\zeta_{\perp}) = \frac{\mu_o}{1 + \gamma_s \zeta_{\perp}^2} \quad (21.b)$$

where μ_o and γ_s are constants. In fact, the channel mobility can be modeled by the Schwarz empirical formula, when we neglect the effect of generated surface states [66]:

$$\mu_n(\zeta_{\perp}) = \frac{670}{1 + (1.49 \times 10^6 \zeta_{\perp})^{1.66}} \text{ cm}^2/\text{V.s} \quad (21.c)$$

Another model, due to Schwarz and Russek[67], considers the channel broadening quantum effects and expresses the channel drift mobility as follows:

$$\mu_c(\zeta_{\perp}) = \frac{\mu_b}{1 + \alpha_s \mu_b \zeta_{\perp} / (1 + \beta_s \zeta_{\perp}^{2/3})} \quad (21.d)$$

where α_s and β_s are constants. The effective vertical field ζ_{\perp} is sometimes related to the surface potential and may be approximated by the following relation, for MOSFETs with n+ polysilicon gate under strong inversion conditions [68]:

$$\zeta_{\perp} \approx \left(\frac{\epsilon_{ox}}{\epsilon_{si}} \right) \left(\frac{V_G + V_T}{2x_{ox}} \right) \approx \frac{V_G + V_T}{6x_{ox}} \quad (22)$$

where ϵ_{si} and ϵ_{ox} are the dielectric constants of silicon and gate oxide, V_G , V_T and x_{ox} are the MOSFET gate voltage, threshold voltage and gate oxide thickness, respectively.

A more elaborate and universal field-dependent mobility model, which reproduces the measured mobility data of

Takagi et al.[69] at the surface of semiconductor devices is given by Darwish et al.[70]. According to Darwish's model, the total carrier mobility is expressed by an equation similar to the scaled Hansch-Murrata model (21.a), with μ_b is given by:

$$\mu_s^{-1}(\zeta_{\perp}) = \mu_b^{-1} + \mu_{sr}^{-1} + \mu_{ac}^{-1} \quad (23.a)$$

Here μ_b is again the bulk mobility, μ_{sr} is the carrier mobility limited by surface roughness and μ_{ac} is the carrier mobility limited by surface acoustic phonons. In the later model, the bulk mobility, μ_b , is expressed by the klassen model[58], the surface acoustic, μ_{ac} , follows the Lombardi model[71]:

$$\mu_{ac}(\zeta_{\perp}) = \frac{B}{\zeta_{\perp}} + \frac{C}{T} \cdot \frac{Dop}{\zeta_{\perp}^{1/3}} \quad (23.b)$$

where B and C are constants ($B=3.61 \times 10^7$ cm/s for electrons and 1.51×10^7 cm/s for holes, $C=1.7 \times 10^4$ cm^{14/3}/V^{2/3}.K for electrons and 4.18×10^3 cm^{14/3}/V^{2/3}.K for holes) and the surface roughness limited mobility, μ_{sr} , is given by:

$$\mu_{sr}(\zeta_{\perp}) = \frac{\delta}{\zeta_{\perp}^{\gamma}} \quad (23.c)$$

where δ and γ are constants, depending on the technology ($\delta \approx 3.58 \times 10^{18}$ V/cm for electrons and 4.1×10^{15} V/cm for holes, $\gamma \approx 2.0-2.9$)

5.2. Impact Ionization Rate

The generation by impact ionization is one of the most important mechanisms limiting the performance of semiconductor devices in general and the submicron MOSFETs in particular. In fact, the electron-hole pair generation by impact ionization, G_{ii} , influences so many characteristics of semiconductor devices such as the breakdown voltage and hot carrier injection currents. The impact ionization mechanism was identified, about 50 years ago, by McKay[72]. Since then, the literature of the impact ionization mechanism has been extensive, e.g. [73-108], but only a few reviews are available. The generation rate by impact ionization G_{ii} has been always expressed in terms of Townsend coefficients (or ionization rates of electrons and holes), α_n , α_p , as follows:

$$G_{ii} = \alpha_n n v_n + \alpha_p p v_p = \alpha_n |J_n| / e + \alpha_p |J_p| / e \quad (24.a)$$

In the DDM, the impact ionization rates are conventionally expressed as functions of the local electric field. For instance, Wolff[73] used the first two terms of the Legendre expansion of the momentum distribution function, and derived the following electron impact ionization rate:

$$\alpha_n(\zeta) = \alpha_{n0} \exp[-C / \zeta^2] \quad (24.b)$$

where α_{n0} and C are constants. According to Baraff[74], this procedure is only justifiable at very high electric fields where electron-phonon collisions are frequent and the momentum distribution function is isotropic. Also, Keldish [75] solved analytically the BTE at high energy assuming parabolic band structure and calculated the impact ionization rate using the symmetric part of the distribution function. The Keldish solution attracted the attention because it tends to the Wolff

relation ($\exp[-C/\zeta^2]$) at high fields and tends to a simple exponential $\exp[-C'/|\zeta|]$ (where C' is another constant) at moderate fields, which coincides with the experiment. In fact, the measurements of Chynoweth[74], Lee et al[77], Van Overstraten and Deman[78], Kotani and Kawazu[79], Maes[80] and Takayangi[81] showed that the impact ionization rate at moderate fields follow a simple exponential function. According to **Grant's** model[82], the electron impact ionization rate follows the following exponential relation:

$$\alpha_n(\zeta) = \alpha_{no} \exp[-\zeta_{cn} / |\zeta|] \quad (24.c)$$

where ζ_{cn} is the critical field at the onset of impact ionization. Shockley tried to find out an explanation of this experimental exponential relation in his study of p-n junctions breakdown[83]. According to Shockley, the impact ionization mechanism is mainly due to streaming of "lucky" electrons which can escape from collisions, and hence the ionization rate of such electrons can be expressed as follows:

$$\alpha_n(\zeta) = \alpha_{no} \exp[-d / \lambda_{op}] \quad (24.d)$$

where $d = (E_n^{th}/e\zeta)$ is the minimum path an electron should travel to gain the threshold energy and λ_{op} is the mean free path between collisions with optical phonons. This model has been utilized to describe the breakdown phenomenon as well as the hot carrier injection and leakage currents in MOSFET devices in DDM-based simulation for long time[84-85]. Unfortunately, the parameters of the lucky-electron exponential model are dispersed among the different measurements of different authors in the literature[84]. In fact, the impact ionization phenomenon happens when drifting electrons have enough energy to ionize the valence electrons of lattice atoms. As the electron energy depends on the whole path of the electron under the effect of both the electric field and collisions, the local electric field value cannot directly reflect the real value of its energy. Thus, the local electric field dependent models of the impact ionization are not physically adequate, and their success in certain classic cases is due to their adjustable parameters. However, with the advent of the hydrodynamic model for semiconductors, where the carrier energy distribution is available, several authors tried to express the impact ionization rates in terms of the carrier mean energy or temperature.

5.2.1. Schöll-Quade Impact Ionization Model

The model of Schöll and Quade[87-88] for impact ionization rate is based on the heated Maxwellian approximation for the symmetric part of the distribution function. According to this model, the impact ionization rate of electrons is given by:

$$\alpha_n(\omega_n) = \frac{I}{v_n^{sat} \tau_o \sqrt{\pi}} \left[\sqrt{\omega_n} \cdot \exp\left(-\frac{I}{\omega_n}\right) - \sqrt{\pi} \cdot \operatorname{erfc}\left(\frac{I}{\sqrt{\omega_n}}\right) \right] \quad (25)$$

where $\omega_n = k_B T_n / E_n^{th}$, E_n^{th} is the electron ionization threshold energy, τ_o is a constant ($\tau_o = \epsilon_o^2 \hbar^3 \pi^3 / 3 e^4 m_n^* \approx 0.0126$ fs) and $\operatorname{erfc}(x)$ is the complementary error function. Note that this model considers a parabolic energy band (constant effective mass m_n^*). In order to get adequate results at moderate fields,

both E_n^{th} and τ_o are usually considered as adjustable parameters, with values which are extremely far from their physical meaning. For instance, **Souissi** et al[89] considered $E_n^{th} \approx 4$ eV and $\tau_o \approx 0.14$ fs, in order to fit this model with experiment.

5.2.2. Baccarani & Stork Impact Ionization Model

The model of Baccarani and Stork belongs to the category of semi-empirical models, which are based on the Shockley lucky-electron model. According to Baccarani and Stork[90], the rate of impact ionization is given by:

$$\alpha_n(\omega_n) = c \lambda_w \cdot \exp\left(-\frac{3\lambda_w}{5\lambda_{op}} \frac{E_n^{th}}{(\omega_n - \omega_o)}\right) \quad (26)$$

where c , λ_w , λ_{op} and E_n^{th} are constants. According to Baccarani and Stork, the ionization threshold energy $E_n^{th} = 1.1$ eV, the energy relaxation length $\lambda_w = (5/3) v_n^{sat} \tau_{ono} = 500$ Å, the mean free path between optical phono collisions $\lambda_{op} = 65$ Å and the adjustable parameter c is equal to 2×10^{12} cm⁻². However, Souissi et al.[89] used the model of Baccarani and Stork in their investigation about impact ionization in bipolar transistors and found that the best fit with measured values implies $E_n^{th} = 5.077$ eV. It has been shown in the latter work that both the Schöll-Quade and Baccarani-Stork models may be used to predict the multiplication factor ($M = \int \alpha_n dx$) across the base-collector zone with reasonable error, only over a limited range of applied bias.

5.2.3. Non-Maxwellian Distribution Function-based Impact Ionization Models

In order to get rid of the disadvantages of the above mentioned models, some authors tried to calculate the impact ionization rate as a function of carrier energy, starting from its microscopic definition, on the basis of non-Maxwellian distribution functions[91-98]. For instance, Matsuzawa, Komahara and Wada[90] suggested the following form for the hot carrier tail of electrons distribution function:

$$f_n(E_n) = C_1 \exp[-1/2 (E_n / k_B T_n)^{3/2}] \quad (27.a)$$

where C_1 is a constant. Also, Sonoda et al.[96] and later **Grasser** et al[97] assumed the following two-components distribution, to account for both cold and hot carriers populations in nanoscale MOSFET devices:

$$f_n(E_n) = C_1 \exp[-(E_n / E_{ref})^b] + C_2 \exp[-(E_n / k_B T_n)] \quad (27.b)$$

where C_1 , C_2 , E_{ref} and b are adjustable parameters, which are used to tune the hot carrier distribution component, and the cold carrier (Maxwellian) component, in order to obtain reasonable results over a wide range of carrier energies. Therefore, when $C_1 = 0$, the distribution function becomes a heated Maxwellian and when $C_2 = 0$ it tends to the tail distribution function. Using this four-parameters distribution function and assuming parabolic energy bands, Morris, Pass and Abebe introduced a simple formulation for the impact ionization rate on the basis of Gauss-Laguerre approximation [98].

It should be noted that several efforts have been devoted for the development a nonlocal impact ionization model on

the basis of the hot-electron subpopulation, e.g.,[99]-[100]. T-W.Tang and Nam have introduced a simplification of such hot-carrier subpopulation models[101]. The impact ionization coefficient is then fitted to homogeneous MC simulation in the bulk of Si as follows:

$$\alpha_n(\omega_n) = 9.59 \times 10^5 \exp[-(134/E_{ref})] \quad (28)$$

for $\omega_n > 0.164 \text{ eV} = 1.156 \times 10^6 \exp[-(90/E_{ref})]$ elsewhere

5.2.4. Advanced Impact Ionization Model

Unfortunately, the success of the above mentioned energy-dependent models of impact ionization is limited to specific cases at small and moderate fields. In addition, these models make use of a number of adjustable parameters, whose fitting values have sometimes irrelevant physical meaning. We think that one source of errors is their lack to a link with the realistic band structure of the semiconductor material. The following phenomenological model accounts for the energy band structure and can be used, with no need to curve fitting of its physical parameters[102].

$$G_{ii} = (n/\tau_{in}) + (p/\tau_{ip}) \quad (29.a)$$

where $1/\tau_{in}$ and $1/\tau_{ip}$ are the electron and hole average ionisation rates. Starting from the scaled form of the impact ionization rate, according to the Thornber theory[103]:

$$\alpha_n(\zeta) = (1/v_n \tau_{in}) \exp[-\zeta_c / \zeta^{1/2} (1 + \zeta^{1/2} / \zeta_p) + \zeta_T] \quad (29.b)$$

where ζ_T , ζ_p and $\zeta_c = E_n^{th}/e\lambda_{op}$ are the critical fields at which the electrons surmount acoustic phonons, optical phonons and impact ionization scattering thresholds. Assuming that the ionization rate can be fully described by the kinetic moments (like, v_n and ω_n), one can write the energy conservation equation (10-c) in the following form in static field conditions:

$$e n \zeta \cdot v_n = -(\partial n / \partial t)_{col} \approx n(\omega_n - \omega_o) / \tau_{in} - (\omega_n - \omega_o)(n - n_o) / \tau_n + n(\omega_n - \omega_o) / \tau_{on} \quad (29.c)$$

where the first term represent the generation by impact ionization, the second term represents the loss of electron energy due to recombination (τ_n being the electrons lifetime and n_o is the equilibrium electron density) and the third term represents the loss of electron energy due to collisions with optical phonons. The second term may be dropped from the above equation because $\tau_{on} \ll \tau_n$. Also the the first and third terms can be combined, with an effective energy relaxation time, which includes the effect of impact ionization at high energies. In fact, this effect is not significant, according to Schöll and Quade[88]. Substituting the product $e \zeta \cdot v_n$ from (27-c) into (27-b), we get the following expression for the electron ionization rate at moderate and high fields:

$$\alpha_n(\omega_n) = \frac{1}{\tau_{in} v_n} = \frac{(\omega_n - \omega_o)}{\tau_{in} v_n E_n^{th}} \cdot \exp\left[-\frac{\eta_n E_n^{th}}{(\omega_n - \omega_o)} \left[\frac{E_p}{E_p + (\omega_n - \omega_o)}\right]\right] \quad (30.a)$$

where $\eta_n = (v_n \tau_{wn} / \lambda_{op})$, λ_{op} is the electron mean free path between optical phonon collisions and E_p is the mean optical phonon energy. At low and moderate fields, this model can be approximated to the following simple form:

$$\alpha_n(\omega_n) = \alpha_{no} \cdot \exp\left[-\frac{E_n^{th}}{\omega_n - \omega_o}\right] \quad (30.b)$$

where $\alpha_{no} \approx \omega_n / (E_n^{th} \tau_{wn} v_n^{sat})$ is the asymptotic value of impact ionization rate and $E_n^{th} \approx E_n^{th} (\tau_{wn} v_n^{sat}) / \lambda_{op}$ is the mean ionization threshold energy for electrons. However, at high fields the impact ionization rate is proportional to $\exp(-E_n^{th} E_p / \omega_n^2)$. Note that we consider $\tau_{wn} = \tau_{wn}(\omega_n)$ and $\lambda_{op} = \lambda_{op}(\omega_n)$. So, even at low fields the exponential relation $\exp(-E_n^{th} / (\omega_n - \omega_o))$ does not imply a Maxwellian distribution because E_n^{th} is energy dependent. The energy dependence of the energy relaxation time, which implicitly includes the energy band structure effects, can be obtained from MC simulation or by measurement as indicated in the next section IV-C. Unlike classical models, the hard threshold energy (E_n^{th}) is replaced with a soft (energy-dependent) mean threshold energy (E_n^I) in our model. This coincides with Bude and Hess conclusions about the impact ionization soft threshold[102]. The calculation of λ_{op} as a function of the electron energy may be carried out by MC simulation in the bulk, using the relation[105]:

$$\lambda_{op}(\omega_n) = \langle u_n(k) / \Gamma_n(k) \rangle \quad (31.a)$$

where $\Gamma_n(k)$ is the total scattering rate by optical phonons. It may be also estimated from the so-called lucky-electron exponential model LE-EM[86]. In our analysis we used the following phenomenological relation, which is based on Crowell and Sze model[106], at the carrier temperature:

$$\lambda_{op}(\omega_n) = \lambda_o \tanh[E_p / 2k_B(T_n - T_L)] \quad (31.b)$$

where λ_o is mean free path between collisions at low fields (when $T_n \approx T_L$). Figs. 3(a) and (b) depict the variation of λ_{op} and α_n in Si, according to the above relations. In our calculations, we took $E_p = 60 \text{ meV}$ and $\lambda_o = 1000 \text{ \AA}$ and exponentially extrapolated the available MC data of $\tau_{wn}(\omega_n)$, as shown in figure 4(a). For the matter of comparison, we plotted α_n according to Baccarani-Stork and Scholl-Quade models, beside our model. The Scholl-Quad model produces excessively high rates when the physical value of τ_o is taken into account. So, we set τ_o equal to 12.6fs, about 3 orders of magnitude greater than its physical value[86]. Note that the value of α_n in our scaled model is greater than all other models and continues to increase at high energies. In fact, the experimental values of α_n may exceed 10^6 cm^{-1} . For instance, the measurement of Kotani and Kawazu of $\alpha_n(\zeta)$ is usually fitted with $\alpha_{no} \geq 10^6 \text{ cm}^{-1}$ [79]. Also, the homogeneous MC simulation[105], indicates that the impact ionization pre-exponential is almost 10^6 cm^{-1} at high energies, as depicted by equation (26). It worth noting that the impact ionization rate at high energies (in the saturation region) is greatly influenced by the roll-off of the enrgy relaxation time, while E_n^{th} and $\lambda_{op}(\omega_n)$ have a relative influence at low and medium energies. This explains the failure of the previously suggested models, to properly estimate α_n at high energies, even with adjusting E_n^{th} and the pre-exponential factors with non physical values, while fixing both λ_{op} and τ_{wn} . For the matter of verification, Figure 14 depicts the I-V characteristics of a reverse biased p-i-n diode near avalanche, with different transport approaches (the DDM, the classic HDM with Scholl-Quade model and our proposed HDM model). As shown, the I-V characteristics obtained by our

model are softer and the breakdown voltage is smaller and more realistic than the classic HDM results.

5.2.5. Energy Broadening of Impact Ionization Threshold

The determination of the impact ionization threshold has been a subject of extensive research, both theoretically and experimentally[107]. In fact the measured values of the ionization threshold and those used in the theoretical models vary widely. As we pointed out in the last section, the mean ionization energy E_n^I in our model of impact ionization has a soft distribution around E_n^{th} . In order to evaluate the broadening of mean ionization energy, we define ΔE_n^I as follows:

$$(\omega_n) = |E_n^I(\omega_n) - E_n^{th}| = E_n^{th} |1 - v_n \tau_{wn} / \lambda_{op}| \quad (32)$$

Figure 3(c) depicts the ionization energy broadening ΔE_n^I as a function of mean electron energy. This broadening is mainly due to the variation of the energy relaxation time and the mean free path at high energies. Curiously, one may wonder if there is any reason to *relate* this phenomenon with the broadening in energy levels due to finite lifetime of energy states between scattering events at high energy[108-109]. In fact, it has been shown experimentally in[110] that there exists a line broadening transition, representing the transition from phonon scattering dominated to impact ionization dominated transport not only in silicon but also in any material with a bandgap. In addition, some theoretical studies of the impact ionization on the basis of quantum transport showed that a fixed impact-ionization threshold does not exist, and the impact-ionization scattering rate is drastically enhanced around the semiclassical threshold by the intracollisional field effect[111]. Of course, the broadening factor may be better evaluated by precise MC simulation, taking into account the impact ionization

mechanism. However, with our simple model of $\lambda_{op}(\omega_n)$ and the exponentially extrapolated $\tau_{wn}(\omega_n)$, we found that ΔE_n^I is centralized around a minimum (almost zero) at $\omega_n \approx 1.8\text{eV}$, which is interestingly equal to $3/2 E_n^{th}$. It should be noted here that we chose $E_n^{th} = E_g \approx 1.2$ and chose $\lambda_0 = 1000\text{\AA}$, such that the distribution of $\lambda_{op}(\omega_n)$ is as close as possible from the experimental LE-EM curve. As shown in figure 3(a), the two curves almost intersect at $\omega_n = E_n^{th} = 1.2\text{eV}$.

5.3. Carrier Energy Relaxation Time

The choice of the energy relaxation time is crucial in the HD simulation because it influences both the static and dynamic characteristics of the device to be simulated. According to the hydrodynamic theory, the exact modelling of the carrier energy relaxation time (and all other relaxation times) should be expressed as function of all the carrier moments like n , v_n and ω_n , etc[112]. However, as we usually truncate the series of moments and satisfy ourselves with the few first moments, it is believed that much of the information about the energy relaxation time is related to the carrier mean energy and density[30]. According to Jacoboni and Reggiani[112], the energy relaxation time should decrease at high fields in a phenomenological way representing the tendency of the isotropic part of the distribution function to decay towards its equilibrium value. So, the later authors used the following equation, to evaluate the carrier energy relaxation time for warm electrons:

$$\tau_{wn}(\omega_n) = (\omega_n - \omega_0) / e v_d \zeta \quad (33.a)$$

This relation, which is sometimes called the Seeger formula[114], reflects the energy continuity at steady state:

$$\partial \omega_n / \partial t = e v_d \zeta + (\partial \omega_n / \partial t)_{col} = e v_d \zeta - (\omega_n - \omega_0) / \tau_{wn} = 0 \quad (33.b)$$

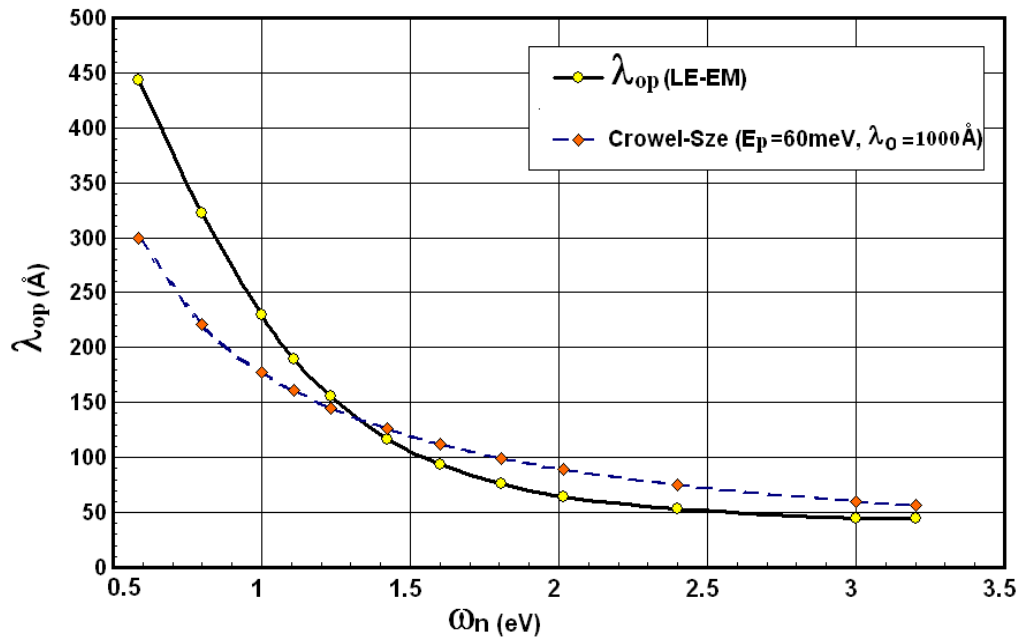


Figure 3(a). Electron mean free path between optical phonon collisions in Si at 300K, according to the lucky-electron exponential model (LE-EM), after[69], and according to the Crowell-Size model[85] at the electronic temperature

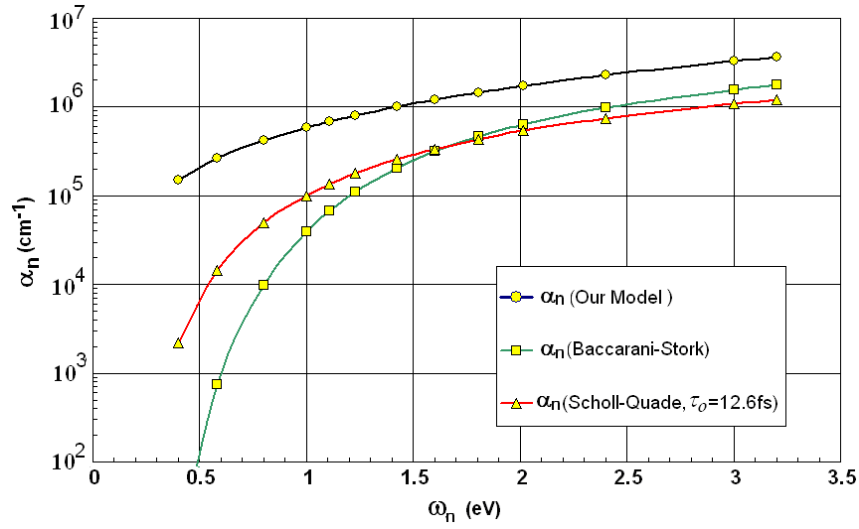


Figure 3(b). Electron impact ionization rate in Si at 300K, as a function of average electron energy, according to Baccarani-Stork model ($\lambda_o=500\text{\AA}$, $\lambda_{op}=65\text{\AA}$), Scholl-Quade model ($\tau_o=12.6\text{fs}$). In all models $E_n^{\text{th}}=1.2\text{ eV}$

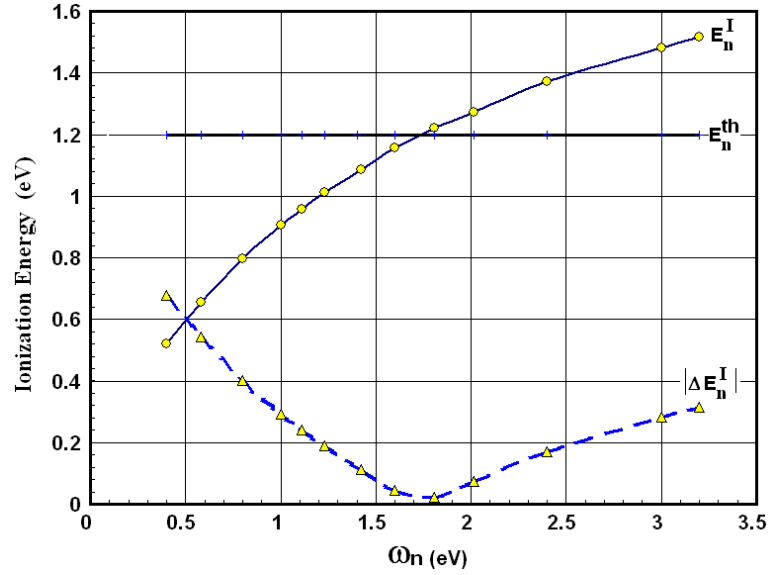


Figure 3(c). Average ionization energy in Si at 300K, according to our model model ($\lambda_o=1000\text{\AA}$, $E_n^{\text{th}}=1.2\text{ eV}$)

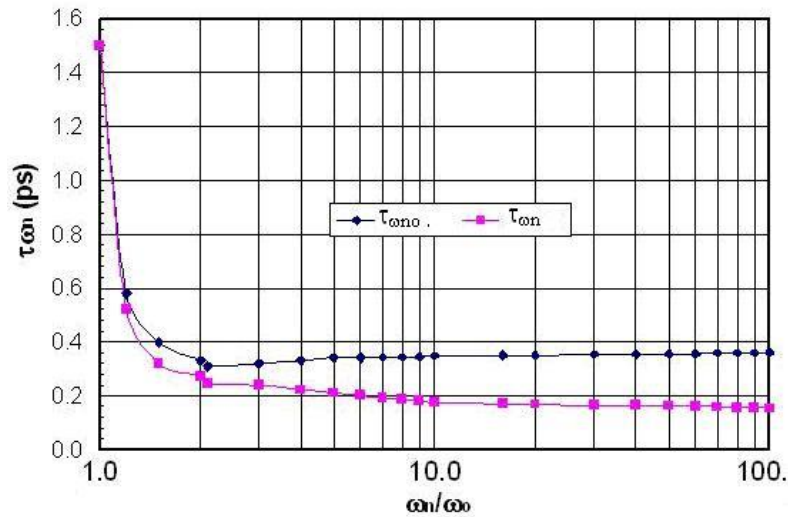


Figure 4(a). Variation of the electron energy relaxation time with electron average energy in Si at 300K, according to MC simulation. In the above curve, the energy bands are assumed parabolic. The lower curve takes the non-parabolicity of the conduction band into account (non-parabolicity factor 0.5V^{-1})

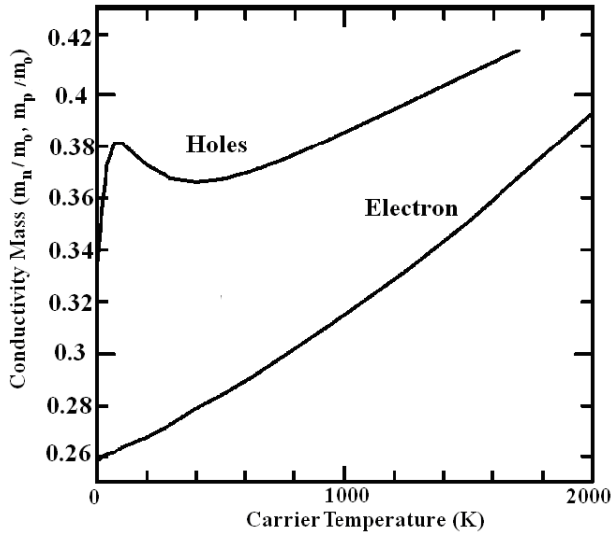


Figure 4(b). Experimental value of electron and holes conductivity mass, after Rife[95]

According to Seeger's static formula, the energy relaxation time can be determined by substituting the static field relations $v_d(\zeta)$ and $\omega_h(\zeta)$ from MC simulation[115]. Gonzalez et al. employed this relation to calculate the fitting parameters of their energy relaxation time model[116]. On the other hand, several authors considered the energy relaxation time as a constant when the electron distribution function is warm enough and the electron velocity tends to saturate. This is a good approximation when the band structure of the material is parabolic. For non-parabolic bands, the energy relaxation time continues to decrease when electron energy is further increased, as shown in Figure 4(a). In fact, it has been shown that the value of the energy relaxation time greatly influences the hydrodynamic simulation results in deep submicron transistors[117]. This is due the fact that the intervalley phonons becomes more effective in dissipating the electron energy at high energies, which lead to decreasing the electron energy relaxation time, at higher energies. For accurate modelling of the energy relaxation time, we propose the following phenomenological relation between the electron average effective mass m_n and τ_{wn} , for energies above the equilibrium value ($\omega_h > \omega_b$):

$$\tau_{wn}(\omega_h) = \tau_{wno} [m_{no} / m_n(\omega_h)] \quad (34)$$

where m_{no} is the density of states effective mass at the bottom of the conduction band (near equilibrium). This model is based on the physical fact that heavy electrons relax faster than lighter ones. In fact, the increased electron-phonon coupling at high fields (where the electron is said to be *dressed* in a cloud of phonons) leads to a modification of electron states and changes their energy (by addition of the self energy) and this increases the mass of electrons and makes their motion slower. Therefore, at high energies where the electron average mass increases as electron energy

increases, the electron dissipates energy more efficiently and the energy relaxation time is shorter. According to the proposed relation, we only need the knowledge of the low-field value of the electron energy relaxation time τ_{wno} and the average mass as a function of electron energy $m_n(\omega_h)$ to obtain $\tau_{wn}(\omega_h)$. The low-field value of the average electron mass, m_{no} , is equal to the conductivity effective mass at the conduction band edge, and can be measured using the optically-detected cyclotron resonance (ODCR). The ODCR method is more accurate than the classical CR and has been recently used to measure the effective mass of several semiconductor compounds[118]. According to the optical measurements of Rife[119] the conductivity effective mass at 300K $m_{no} = 0.275m_0$ and $m_{no} = 0.365m_0$ as shown in figure 4(b). The ultrafast laser based pump-probe techniques have been used to measure the energy relaxation as well as the momentum relaxation times in Si. Using this technique, a time constant of 32 ± 5 fs associated with momentum relaxation and an electron - phonon energy relaxation time of 260 ± 30 fs have been extracted from the coherent-transient variations in (001) Si at 300K[120].

In order to verify our model, we used the MC simulation to calculate the average electron mass as a function of the average electron energy, and compared it with the measured ratio of (m_{no}/m_n), as shown in Figure 5. As shown in figure, the normalized value of the average inverse mass decreases as the electron energy increases. Then we calculated the energy relaxation time $\tau_{wn}(\omega_h)$, using the above phenomenological relation (above ω_b , when electrons start to warm up). As shown in Figure 5, the discrepancy between the the energy relaxation time, according to MC and the calculated values according to our model lies within the measurement error ($\sim 10\%$) for a wide range of carrier temperatures (up to 2000K and may be extrapolated to higher values). Alternatively, our model can be used to calculate the energy dependence of the average electron mass $m_n(\omega_h)$ from the energy dependence of the electron energy relaxation time $\tau_{wn}(\omega_h)$. The energy dependence of τ_{wn} of several semiconductors (e.g., AlGaAs/GaAs, AlGaIn/AlIn/GaN) has been measured using the microwave-noise method[121]. This method is based on the measurement of the noise temperature, which is equal to the electron temperature T_n in the semiconductor, according to the following relation:

$$\tau_{wn} = 3/2 k_B (T_n - T_L) / e v_d \zeta \quad (35)$$

where we neglect the convection part of the electron energy and consider $\omega_h = 3/2 k_B T_n$. However, we have no experimental data yet about the energy relaxation time in Si (as a function of carrier temperature or energy) using this method. So, the proposed model which correlates $\tau_{wn}(\omega_h)$ to the already measurable $m_n(\omega_h)$ should be very useful in this case.

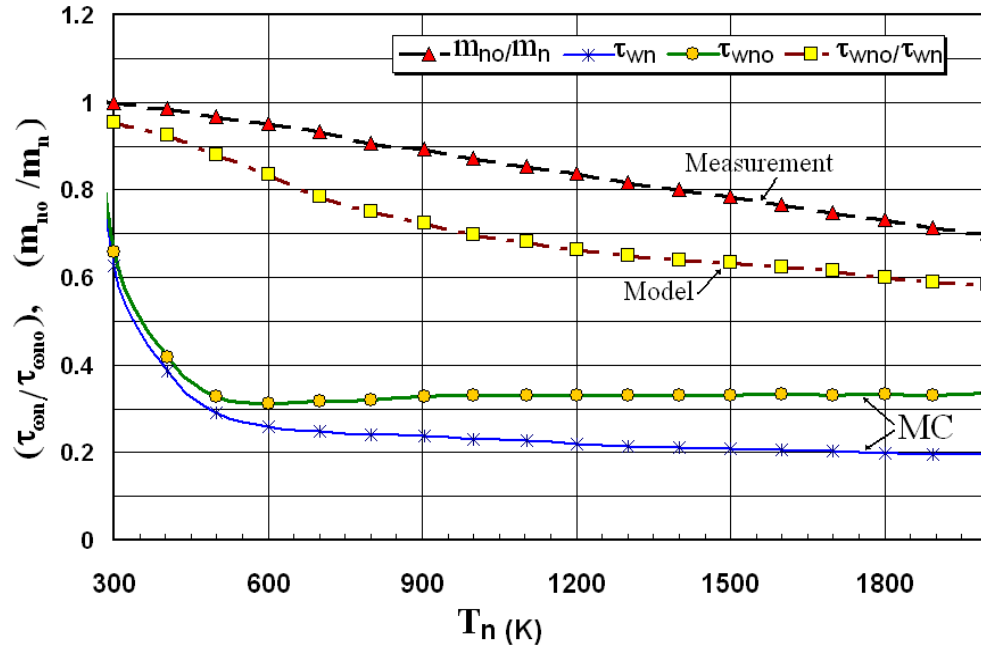


Figure 5. Comparison between the normalized inverse mass (m_{no}/m_n), according to optical measurement[52] and our model. The model is calculated from the normalized energy relaxation time (τ_{cono}/τ_{con}) according to MC data, by our phenomenological relation (25)

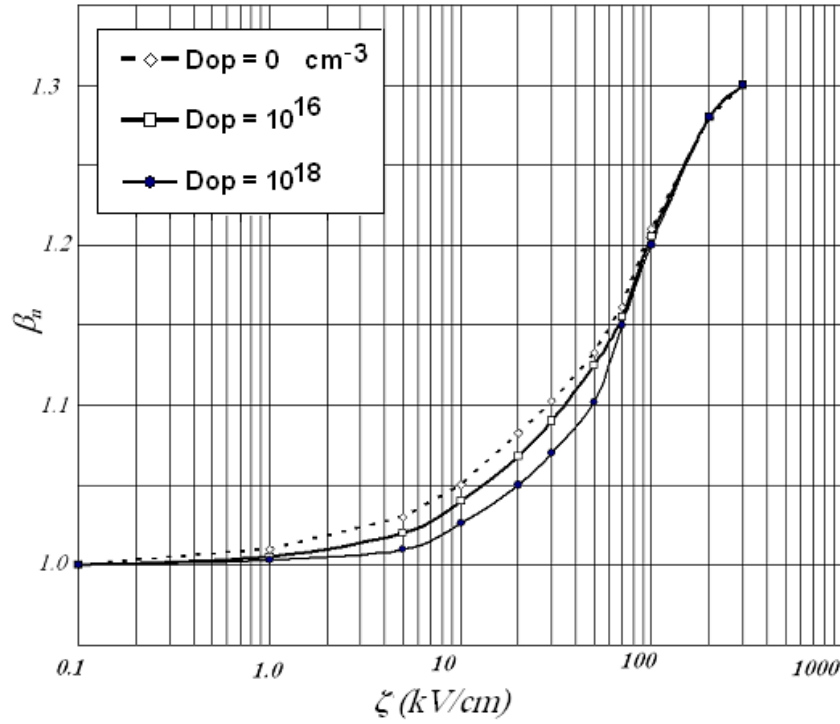


Figure 6(a). Heat flux beta factor in Si at 300K, calculated from MC simulation, with non-parabolicity factor 0.5V^{-1}

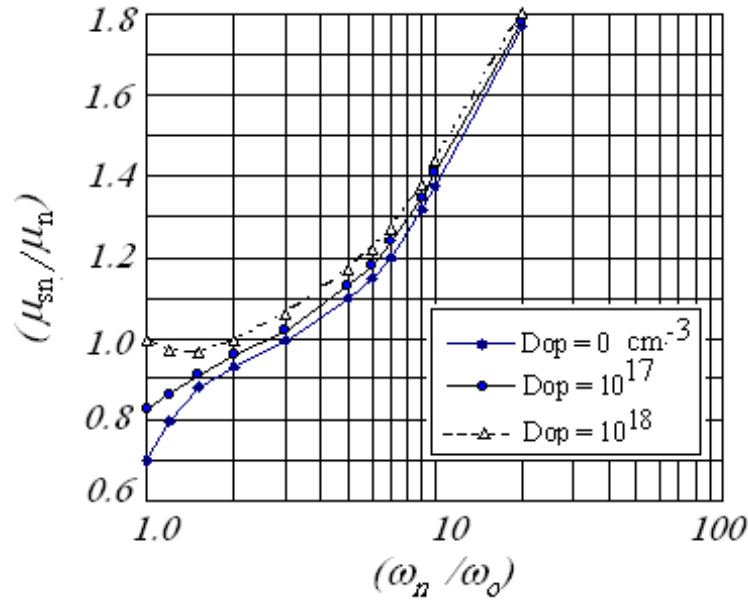


Figure 6(b). Relative energy flow mobility in Si at 300K, calculated from MC simulation, with non-parabolicity factor 0.5V-1

5.4. Advanced Heat Flux Model

As we pointed out earlier, the heat flux term in the majority of previous HDM's was either neglected or modelled by the Fourier relation (12-a). It has been shown that this model is not accurate for modelling the heat flux across semiconductor interfaces in general and p-n junctions in particular[122]-[124]. In order to increase the accuracy of the hydrodynamic model, we propose the following model, which is based on the third moment of the BTE in steady state:

$$nF \cdot \langle (m_n^*)^{-1} E_n + u_n \otimes u_n \rangle + \nabla_x \cdot (n \langle E_n u_n \otimes u_n \rangle) = \left[\frac{\partial S_n}{\partial t} \right]_c \approx - \frac{S_n}{\tau_{sn}} \quad (36.a)$$

where we suppressed the time derivative ($\partial S_n / \partial t$) and used the relaxation time approximation (τ_{sn} is the energy flux relaxation time). The above conservation equation (of energy flux), may be further simplified by approximating the average terms, as follows[123]:

$$\langle (m_n^*)^{-1} E_n + u_n \otimes u_n \rangle \approx 5/2 \alpha_n \langle u_n \otimes u_n \rangle, \quad \langle E_n u_n \otimes u_n \rangle \approx \beta_n m_n \langle u_n \otimes u_n \rangle^2 \quad (36.b)$$

where the correction factor α_n expresses the anisotropy of the distribution function and the correction factors β_n expresses how much the distribution function is deviated from the Maxwellian distribution. These parameters can be estimated by MC simulation in the bulk of semiconductor. Then we can write the energy flux as the sum of a conduction part Q_n and a convection part (where J_n is a multiplier):

$$S_n = Q_n + 5/2 (\mu_{sn}/\mu_n) (k_B T_n) J_n \quad (36.c)$$

Here $\mu_{sn} = (e m_n^{-1} \tau_{sn})$ and the electron heat flux Q_n ($\lim_{J_n \rightarrow 0} S_n$) is given by:

$$Q_n = -k_n' \nabla T_n - k_n'' [\nabla(nT_n) / n] \quad (37.a)$$

with

$$k_n' = 5/2 (k_B^2/e) n \mu_{sn} \beta_n T_n, \quad (37.b)$$

$$k_n'' = 5/2 (k_B^2/e) n \mu_{sn} (\beta_n - \alpha_n') T_n \quad (37.c)$$

Note that the convection energy flux is similar to our 3-moments formulation (11), except for the correction factor (μ_{sn}/μ_n) and that $(\omega_n + k_B T_n)$ is replaced with $5/2(k_B T_n)$. However, we just called the third moment equation in order to derive a more accurate formula of the heat flux term., which contains the effect of both the carrier temperature and the carrier density gradients.

5.5. Modified Wiedman-Franz Relation

If the anisotropy of the distribution function is negligible, we can substitute $\alpha_n \approx 1$. Then the heat flux term can be put in the following simple form:

$$Q_n = -5/2 (k_B^2/e) \mu_{sn} (2\beta_n - 1) \nabla(nT_n) \quad (38.a)$$

Figures 6(a) and (b) depict the electron heat flux beta factor and the relative energy flux mobility (μ_{sn}/μ_n) as a function of electron energy. We calculated these parameters by MC simulation in the bulk of Si at 300K with non-parabolicity factor

0.5V⁻¹. Alternatively, they may be evaluated, as functions of carrier energy, and doping level, by appropriate physical models. For instance, the energy flux mobility may be modelled in much the same way as the drift mobility as follows [124]:

$$\mu_{sn}^{-1} = \mu_{sno}^{-1} [1 + \xi_n (\omega_n - \omega_o)] \quad (38.b)$$

where $\mu_{sno} = \mu_{sno}(Dop)$ is the energy flux mobility at low field and $\xi_n = 5/2 n \mu_{sno} \omega_n / (e \tau_{on} v_n S_n)$. Also, the heat flux beta factor may be approximately expressed as follows in Si at 300K:

$$\beta_n(\omega_n, Dop) = \beta_1 [1 + (Dop / N_1)^{\alpha_1}]^{\alpha_2} + \beta_2 (\omega_n - \omega_o) [1 + (Dop / N_1)^{\alpha_1}] \quad (38.c)$$

where $\alpha_1, \alpha_2, \beta_1, \beta_2$, and N_1 are constants. For Si at 300K with doping levels $Dop \leq 10^{19} \text{ cm}^{-3}$ and electron energy $\omega_n > 0.1 \text{ eV}$, we have: $\beta_1 = 0.9775$, $\beta_2 = 6.464 \text{ eV}^{-1}$, $\alpha_1 = 0.192$, $\alpha_2 = 6.372$, $N_1 = 10^{21} \text{ cm}^{-3}$.

When the carrier-concentration gradient is negligible (with respect to the temperature gradient), the heat flux formula (35-a) can be further reduced to the conventional Fourier relation (12-a), with the following carrier-thermal conductivity:

$$k_n = 5/2 (k_B^2 / e) n \mu_{sn} (2\beta_n - 1) T_n \quad (39.a)$$

The above equation is equivalent to the conventional Wiedemann-Franz relation with the following 'modified' energy- and doping-dependent Lorenz number:

$$\gamma_n = 5/2 (\mu_{sn} / \mu_n) (2\beta_n - 1) \quad (39.b)$$

In the extreme case of very low doping and very low electric field, where $\mu_{sn} = \mu_n$ and $\beta_n = 1$ then $\gamma_n = 5/2$ as compared to $(5/2 + r)$ in the conventional model (12-c). Figure 13 depicts the heat flux as obtained by the classic Fourier relation and the new model. As shown in figure, the consideration of the carrier gradients in the new model broaden and smooth the heat flux profile near junctions.

5.6. Tunneling & Hot Carrier Injection Currents

The tunnelling and hot carriers injection currents play an important role in modern semiconductor devices in general and the ultra short MOSFET devices in particular. There are two tunnelling (through the barrier) mechanisms and four hot carrier injection (over the barrier) mechanisms which are commonly encountered in MOSFET devices, namely:

- Field-assisted (Fowler-Nordheim or **FN**) tunnelling,
- direct tunnelling (**DT**),
- drain avalanche hot carrier injection (**DAHCI**),
- channel hot electron injection (**CHED**),
- substrate hot electron injection (**SHI**) and
- secondary generated hot electron injection (**SGHEI**)

These mechanisms are usually monitored by measuring the gate current, I_G , and the substrate current, I_{sub} . In the following subsections we describe briefly these parameters and how they are modeled within the framework of the hydrodynamic model.

5.6.1. Tunneling Currents

The tunnelling currents are either direct or of field-assisted (Fowler-Nordheim) type. The direct tunnelling can take place at low gate voltages via thin oxides layers (less than 50Å) and has a weak dependence on the gate field. The FN tunnelling is a field-assisted mechanism which is strongly

dependent on the gate field and dominates in modern MOS structures. The gate tunnelling current density is given by the following integration [125]:

$$J_G = \int_0^\infty g_c(E_n) u_{n\perp} f_n(E_n) T(E_n) dE_n \quad (40)$$

where $T(E_n)$ is the tunneling probability, $g_c(E_n)$ is the density of states in the conduction band, $u_{n\perp}$ is the electron group velocity perpendicular to the Si surface ($u_{n\perp} \approx 1/4 u_n$). The integration in the above equation starts from the semiconductor conduction band edge, as a reference. For trapezoidal barrier of upper height ϕ_B and lower height ($\phi_B - V_{ox}$), where V_{ox} is the potential voltage across the insulator gate, the tunnelling probability is usually expressed using the WKB approximation as follows:

$$T(E_n) = \exp \left[-\frac{4\sqrt{2m_{ox}}}{3e\hbar\zeta_{ox}} (e\phi_B - E_n)^{3/2} \right] \quad (41.a)$$

In the upper triangular part of the barrier, where $e\phi_B > E_n > e(\phi_B - V_{ox})$, and

$$T(E_n) = \exp \left[-\frac{4\sqrt{2m_{ox}}}{3e\hbar\zeta_{ox}} ((e\phi_B - E_n)^{3/2} - (e\phi_B - E_n - eV_{ox})^{3/2}) \right] \quad (41.b)$$

in the lower rectangular part of the barrier where $E_n < e(\phi_B - V_{ox})$. Here ζ_{ox} and m_{ox} are the electric field and effective mass of electrons at the insulator (for SiO_2 , $m_{ox} = 0.42m_0$). In the case of the field-assisted Fowler-Nordheim mechanism, we consider the triangular part of the barrier, which is described by (38-a). Assuming the energy distribution function Maxwellian and the energy bands parabolic, we get the following field-dependent gate current density:

$$J_G = J_o \zeta_{ox}^2 \exp[-\zeta_o / \zeta_{ox}] \quad (42)$$

where the J_o and ζ_o are constants, related to the energy barrier height ϕ_B between the insulator and the injecting conductor as follows:

$$\zeta_o = \frac{4\sqrt{2m_{ox}}}{3e\hbar} (e\phi_B)^{3/2} \quad (43.a)$$

$$J_o = \frac{e^2}{16\pi^2 (m_{ox} / m_o) \hbar \phi_B} \quad (43.b)$$

The tunnelling mechanism can be initiated by low energy carriers (near equilibrium). However, it is also possible for hot electrons to tunnel when their energy is not sufficient to surmount the barrier. In order to obtain more realistic results of the gate tunnelling current in short MOSFET devices, some authors assumed a non-Maxwellian distribution function and considered the nonparabolicity of energy

bands[126]. The total gate current may be partitioned between the source and drain, as follows:

$$I_G = I_{GS} + I_{GD} \quad (44.a)$$

where

$$I_{GS} = W \int_0^L J_G \left[I - \frac{y}{L} \right] dy, \\ I_{GD} = W \int_0^L J_G \left[\frac{y}{L} \right] dy \quad (44.b)$$

where W and L are the MOSFET channel width and effective length, respectively. When the substrate bias is high enough, the thermoionic emission across the gate oxide dominates the tunnelling current. The thermoionic emission current can be calculated by a formula similar to equation (40), with replacing the tunnelling probability, T , by the probability that an electron will not scatter in the image potential well in the oxide region, P .

$$I_G = W \int_0^L \int_{\phi_B}^{\infty} g_c(E_n) u_{n\perp} f_n(E_n, y) P(\zeta_{ox}, y) dE_n dy \quad (45.a)$$

with

$$P = \exp\left(-\frac{x_{ox}}{\lambda_{ox}}\right) \text{ for } \zeta_{ox} > 0 \text{ and} \\ P = \exp\left(-\frac{(t_{ox} - x_{ox})}{\lambda_{ox}}\right) \text{ for } \zeta_{ox} < 0 \quad (45.b)$$

where x_{ox} is the gate oxide thickness and λ_{ox} is the mean free path of electrons inside the gate oxide (for SiO_2 , $\lambda_{ox} \approx 32 \text{ \AA}$). In order to account for both tunnelling and thermoionic emission, the above equation should be modified as follows[127]:

$$I_G = W \int_0^L \int_{\phi_B}^{\infty} g_c(E_n) u_{n\perp} f_n(E_n, y) T(E_n) P(\zeta_{ox}, y) dE_n dy \quad (45.c)$$

Finally it should be noted that the Fowler-Nordheim tunnelling gate current may photogenerate e-hole pairs at the substrate and hence it is likely to be the main origin of the substrate leakage current, rather than the anode hole injection[128].

5.6.2. Hot Carrier Injection Currents

The channel hot electron injection (**CHEI**) occurs when the gate voltage is high enough and $V_G \approx V_D$. Channel carriers which are accelerated by lateral fields and transported from the source to the drain may be driven towards the gate oxide before they reach the drain. The drain avalanche hot carrier injection (**DAHCI**) occurs when a high drain voltage is applied in non-saturation mode ($V_D > V_G$) which results in a high electric field near the drain, and hence accelerating channel carriers into the drain depletion region. The accelerated channel carriers collide with Si atoms valence electrons, creating electron-hole pairs by impact ionization. Some of the generated electron-hole pairs are again accelerated and may acquire sufficient energy to

surmount the Si/SiO₂ barrier. The hot carriers that surmount the gate oxide barrier can inject into the gate oxide where they may be trapped and gives rise to a shift in the MOSFET threshold voltage, surface mobility and dynamic conductance. The substrate hot electron injection (SHEI) occurs at high substrate bias, $|V_B| \gg 0$ and strong inversion, usually with both drain and source grounded. Under this condition, carriers of one type in the substrate are driven by the substrate field toward the Si-SiO₂ interface. Carriers can be generated by external optical or thermal excitation. As carriers move toward the substrate-oxide interface, they gain further kinetic energy from the high field in surface depletion region. They eventually overcome the surface energy barrier and get injected into the gate oxide, where some of them are trapped. The secondary generated hot electron injection (SGHEI) occurs under conditions similar to DAHCI, when $V_D > V_G$, which lead to impact ionization of hot carriers. However, SGHEI involves secondary carriers that are created by an earlier incident of impact ionization and driven under the influence of the substrate bias. This bias produces a field that drives hot carriers toward the surface region, where they gain more energy to overcome the gate oxide barrier[124]. The so-called “channel-initiated secondary electron (CHISEL) is a variant of the SGHEI, which relies on ionization feedback and is activated by a negative substrate bias $V_B < 0$. CHISEL is used as a reliable programming technology in recent low-voltage Flash EEPROM devices, with floating gate lengths down to 0.2 μm [131]. Figure 18 illustrates the different hot injection and tunnelling mechanisms in MOSFET devices.

The injection of hot-electrons into the gate-oxide has been usually modelled by the lucky-electron model[83]. According to Hu et al., the probability of a channel electron reaching the gate terminal as a combination of the probabilities of the following events:

- the electron gains sufficient energy in the lateral electric field to overcome the interfacial
- potential barrier and retains this energy after a collision directs its momentum towards the interface,
- the electron reaches the interface without suffering any more collisions, and
- the electron is not scattered back into the semiconductor in the image-force potential well present close the interface

The lucky-electron model, despite of its drastic assumptions, remains the most useful approach to estimate the injection currents with reasonable agreement with experimental results. On the basis of the lucky-electron model, it can be shown that the fraction of the channel carrier supply which is injected into the gate oxide is given by [129]:

$$I_{inj} \propto I_{sub} \exp\left(-\frac{\phi_B}{e\lambda_n\zeta}\right) \quad (46.a)$$

where, ϕ_B is the interfacial potential barrier, λ_n is the electron mean free path and ζ is the effective lateral electric field. It can be shown that the effective barrier potential ϕ_B is given by:

$$\varphi_B = \Phi_B - a\sqrt{\zeta_{ox}} - b\zeta_{ox}^{2/3} \quad (46.b)$$

where Φ_B , a and b are constants, expressing the main barrier height and lowering effects due to image force and quantum tunnelling. For Si/SiO₂ interface, $\Phi_B = 3.2\text{V}$, $a =$ and $b = 2.59 \times 10^{-4} \text{ (Vcm)}^{1/2}$. As the substrate current is generated due to impact ionization in the lateral electric field close to the drain, it is linearly proportional to the drain current. On the basis of the lucky-electron concept, it can be shown that the substrate currents is given by :

$$I_{sub} \propto I_{ds} \int_0^{L_d} \alpha_n dy \quad (47)$$

Where I_{ds} is the drain current, L_d is the length of the pinch-off region and α_n is the electron impact ionization coefficient in the velocity saturated part of the channel. So, the substrate current can be given by:

$$I_{sub} = C.I_{ds} \exp\left(-\frac{E_n^{th}}{e\lambda_n\zeta}\right) \quad (48)$$

where, E_n^{th} is the impact ionization threshold energy for electrons. As seen from this equation, the ratio of the substrate and drain currents provides a direct measure of the average lateral electric field. In addition, this multiplication ratio, is often used as a monitor for the device degradation.

6. Lattice Heat Conservation Equation

Some recent studies demonstrated the important role of lattice heat and thermal activation of the low voltage impact ionization in deep-submicrometer MOSFETs[132]. In addition, the recent studies of silicon on insulator (SOI) devices by the classical HDM, showed certain anomalies due to lack of a heat evacuation mechanism at the insulator interface[133]. Some authors suggested to cure this problem by considering a tensorial temperature and modifying the closure condition for energy flux term [134]. Others authors suggested coupling the lattice heat equation to the set of HD equations[135].

The classical heat diffusion equation, which resolves the temporal and spatial distribution of lattice temperature along the semiconductor, reads:

$$\rho_L c_p \frac{\partial T_L}{\partial t} - \nabla \cdot (k^{\text{th}} \nabla T_L) = \mathbf{H}_s \quad (49.a)$$

where ρ_L is the lattice density, c_p is the lattice specific heat and their product is equal to the heat capacitance ($C_p = \rho_L c_p$) of the semiconductor material. Also k^{th} is the thermal conductivity of the semiconductor and the heat source term \mathbf{H}_s is given by[136]:

$$\mathbf{H}_s = \mathbf{J} \cdot \zeta + (E_c + \omega_n) - (E_v - \omega_p)(G - R) \quad (49.b)$$

where $(E_c + \omega_n)$ is the absolute average electron energy and $(E_v - \omega_p)$ is the absolute average hole energy in the crystal lattice. In Si at 300K, $\rho_L = 0.232 \text{ g/cm}^3$ and $c_p = 7.03 \times 10^4 \text{ cm}^2/\text{Ks}^2$ and their temperature dependence is negligible[137]. We dully note that the carrier thermal conductivity is a small fraction of the Si material thermal conductivity k^{th} because

heat conduction in semiconductors is dominated by phonon transport. It should be also noted that for $T_L > 100\text{K}$, the thermal conductivity in Si is practically independent of doping concentration[138]. The temperature dependence of k^{th} in the bulk of crystalline Si may be modelled according to Glassbenner and Slack[139] as follows:

$$k^{\text{th}}(T_L) = k_o (T_L/300)^{-\alpha} \text{ (W/K cm)} \text{ for } T_L > 100\text{K} \quad (49.c)$$

where $\alpha = 1.2$ and $k_o \approx 1.45$ for Si. However, in thin semiconductor layers the thermal conductivity is reduced due to the phonon scattering process at layer boundaries (the size effect), as described in[140]. An analytical expression describing the thermal conductivity as a function of distance, into thin Si layers can be found in[141]. A more rigorous approach to solve the problem of heat evacuation in SOI devices, consists in solving the BTE for phonons. In fact it is well known that the LO phonons have small group velocities ($\sim 10^5 \text{ cm/s}$) and anharmonically decay into faster acoustic phonons which in turn transport the energy out off the semiconductor device. So, the phonon BTE may be simplified by assuming a two-fluid phonon transport model involving a stationary optical reservoir mode and a propagating acoustic mode. The latter approach may consider not only the heat evacuation by optical phonons, but also their anharmonic decay to 'fast propagating' acoustic phonons. As a compromise between the above mentioned approaches, the a lattice heat continuity equation may be added to the set of HDE's with phonon energy relaxation term. The transformed phonon BTE in the relaxation time approximation reads[142]

$$\frac{\partial \varpi}{\partial t} + \mathcal{G} \cdot \nabla \varpi = -\frac{\varpi - \varpi_o}{\tau_\varpi} + H_s \quad (50.a)$$

where ϖ is the phonon energy per unit volume, v the phonon velocity and τ_ϖ is the phonon energy relaxation time and H_s is the volumetric heat generation rate absorbed from hot electrons, which can be extracted from the solution of the HDE's. According to the kinetic theory, the phonon energy relaxation time is related to the phonon velocity v_{ph} and mean-free path Λ_{ph} , by the following relation[143]:

$$\Lambda_{ph} = v_{ph} \tau_\varpi = \frac{3k_B}{C_p v_{ph}} \quad (50.b)$$

So, the lattice energy conservation equation may be written as follows:

$$\frac{\partial W_L}{\partial t} + \nabla \cdot S_L = H_s - \frac{W_L - W_o}{\tau_\varpi} = R_{\omega L} \quad (50.c)$$

where $W_L = \int C_v dT_L$ is the lattice energy density, W_o is the lattice energy density at equilibrium (at $T_L = T_o$) and $S_L = -k^{\text{th}} \nabla T_L$ is the lattice energy flux (or heat flux). We note that the overall lattice energy conservation dictates the following relation:

$$R_{\omega L} = R_{\omega n} + R_{\omega p} = \zeta \mathbf{J} + (E_g + \omega_n + \omega_p)(G - R) - n(\omega_n - \omega_o)/\tau_{wn} - p(\omega_p - \omega_o)/\tau_{wp} \quad (51.a)$$

where $R_{\omega n}$ is equal to the RHS of the energy conservation equation (10-c) for electrons and $R_{\omega p}$ for holes. When the net

generation-recombination rate is negligible, $R_{\omega L}$ represents the local energy transfer rate from crystal lattice to the electron and hole gas subsystems. Therefore we can write the following correlation function between the charge carriers relaxation times and phonons relaxation time:

$$n(\omega_n - \omega_0)/\tau_{wn} + p(\omega_p - \omega_0)/\tau_{wp} = (W_L - W_0)/\tau_w \quad (51.b)$$

Note that our formulation of the lattice heat conservation equation is tightly coupled with the set of HDEs, via the average electron and hole average energies (which makes part of the heat source term H_s) and the energy relaxation correlation function.

7. Quantum Corrections

The so-called quantum hydrodynamic model (QHDM) can be derived by a variety of methods[144-152], such as the first few moments of the WBTE or using the Madelung transform[147] or the principle of minimum entropy[148]. The formulation of the QHDM usually retains the lowest order (\hbar^2) term in the series expansion of a complicated quantum operator acting on the Wigner distribution function and the system potential energy. From the mathematical point of view, the most significant difference between the semiclassical HDM and the QHDM is the quantum potential term, V_q , which appears in the average energy expression[150]:

$$\omega_n = \frac{1}{2} m_n^{-1} \langle p_n^2 \rangle + \frac{3}{2} k_B T_n + V_q \quad (52.a)$$

where $\langle p_n \rangle$ is the average momentum of electrons and V_q is given by:

$$V_q = - \hbar^2 \nabla^2 [\ln n] / 8m_n \quad (52.b)$$

The quantum potential term is sometimes merged with the electron temperature, to form the so-called quantum temperature T_{qn} :

$$T_{qn} = T_n + \frac{2}{3} V_q/k_B \quad (52.c)$$

The quantum correction appears also in the current equation (which is a reduced form of the momentum conservation equation) in the form of an additional current J_q . The following electron current equation depicts this correction term[151]:

$$\mathbf{J}_n (\text{quantum}) = \mathbf{J}_n (\text{semiclassical}) + \mathbf{J}_q \quad (53.a)$$

with

$$J_q = n\mu_n \left(\frac{\hbar^2}{6m_n^*} \right) \cdot \nabla \left(\frac{\nabla^2 \sqrt{n}}{\sqrt{n}} \right) \quad (53.b)$$

Note that the quantum correction term is significant when the electron concentration n varies so rapidly over small distances in the order of de-Broglie wavelength (\hbar/p). Adding the quantum correction term in this manner is sometimes referred to as the density gradient (DG) method. The DG theory has been used to model the quantum confinement as well as the tunnelling currents in MOS devices[152].

8. Quasi-Ballistic Transport Considerations

It has been shown that the operation of sub 0.1 micron MOSFET transistors is quasi-ballistic, in a small portion of the channel[153-158]. Some authors shows that quasi-ballistic transport in nano-transistors takes place near the source region and others showed that quasi-ballistic transport and back scattering take also place near drain region as well[157]. In all cases, one should be aware that even when the transport is full ballistic, the contact resistance of the device is still there limiting the transport process. However, the quasi-ballistic transport can be also considered within the framework of the semiclassical theory[156]. In fact, it has been shown that semiclassical transport models along the MOSFET channel may remain reliable down to 10nm[157]. In addition, it has been shown in the latter article, that the semiclassical model is more reliable than the quantum simulation, even when the ratio of coherent transport along the MOSFET channel is not negligible (down to 10nm). Figure 7 depicts the electron velocity distribution along a 50nm n-i-n structure, in the ballistic mode and using different transport approaches.

9. Sample of Simulation Results

Figure 1 depicts the electron temperature T_n , according to Monte Carlo simulation, the classic HDM and according to our definition. As shown in figure, the electronic temperature is reasonably estimated using our model when taking $g_n \approx 1$, for electric field up to 200 kV/cm. For the matter of demonstration of the proposed HDM and comparison with other DDM-based simulation, we simulated the carrier transport across a reverse-biased silicon p-i-n diode. The simulated diode is 100 μ m long and has a p^+ side with Gaussian distribution and peak doping of 10^{19}cm^{-3} , as shown in Figure 8. The diode base n-layer is homogenously doped with 10^{14}cm^{-3} , and the metallurgical junction is almost at 11 μ m apart from the p^+ contact. Figures 9 and 10 depict the two-dimensional distributions of electron and hole density and temperatures inside the p-i-n diode at 75V reverse bias. Figures 11 and 12 depict the one-dimensional distributions of electron and hole density and temperature along the p-i-n diode at 500V reverse bias. Also figures 13 and 14 depict the one-dimensional distributions of electron and hole energy flux and heat flux along the p-i-n diode at 500V reverse bias. In addition, Figure 15 shows the I-V characteristics of the simulated diode near breakdown. We discussed in[159] the effect of the hydrodynamic simulation on the distribution of charge carriers and showed that discrepancy from the DDM-based results is due to the carrier thermal back diffusion. In order to show the important role of the energy relaxation time model in the HD simulation, we traced the electron distribution across the p^+ -n junction at various values of the τ_{wn} . Figure 16 depicts the electron density distribution along a reverse biased p-i-n diode at three values of the energy relaxation time. Note that the electron distribution, which is obtained using the HDM with lower τ_{en} tends to the DDM classical distribution. This

means that for shorter energy relaxation times, the electrons are more efficient in dissipating their energy. For the limiting case when τ_{en} tends to zero, the electrons will tend to dissipate their gained energy at once and their average energy is equal the lattice energy ω_b . This is exactly the case of the DD simulation, where we consider the electron temperature equal to the lattice temperature ($T_n = T_L$) at all fields.

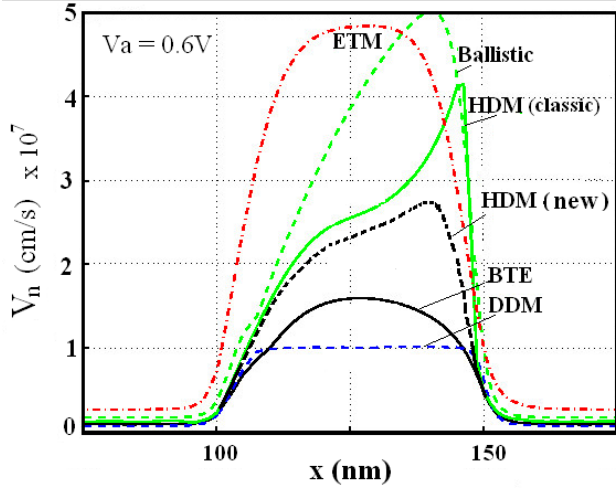


Figure 7. Effect of quasi-ballistic transport on the electron velocity across an n-i-n diode, according to several models[118]

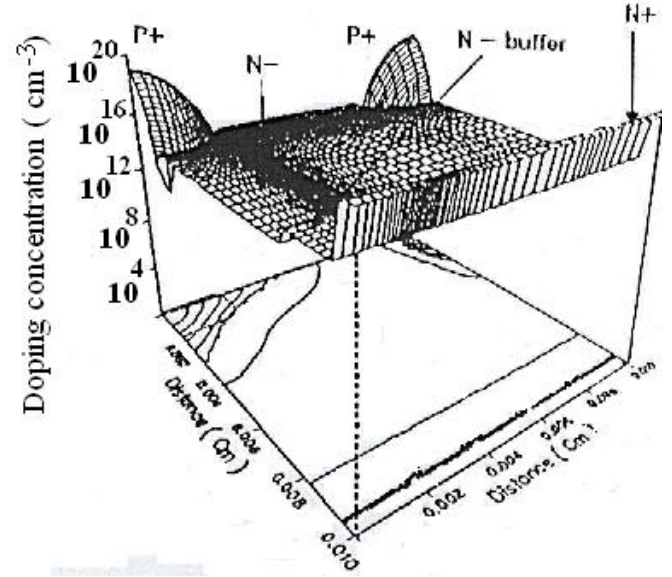


Figure 8. (a) Two-dimensional doping profile of the simulated p-i-n diode

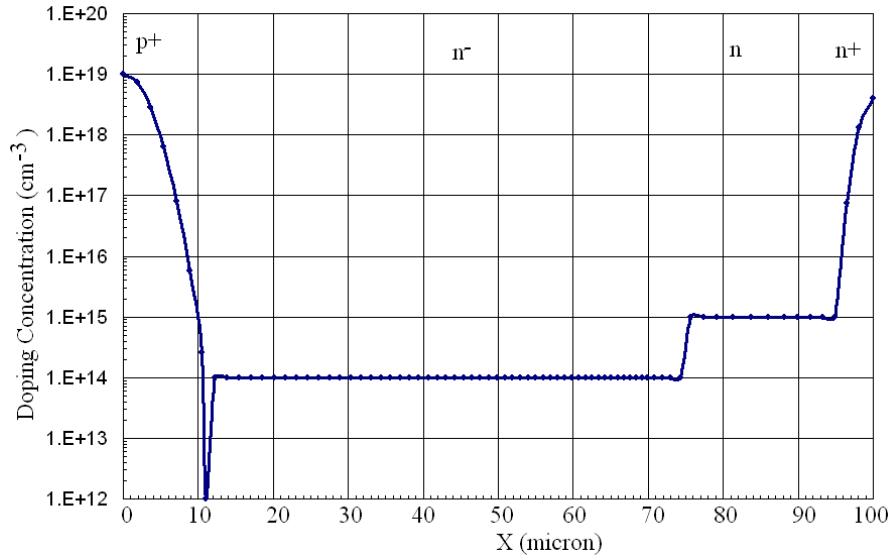


Figure 8. (b) Lateral doping profile along the x-axis of the p-i-n diode

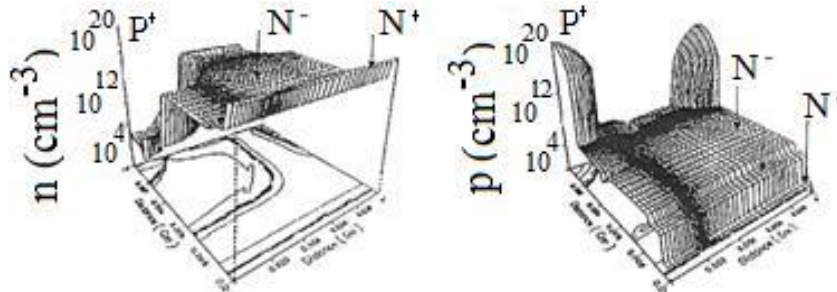


Figure 9. (a) Electron and (b) hole density distribution in the p-i-n diode (at -75V bias)

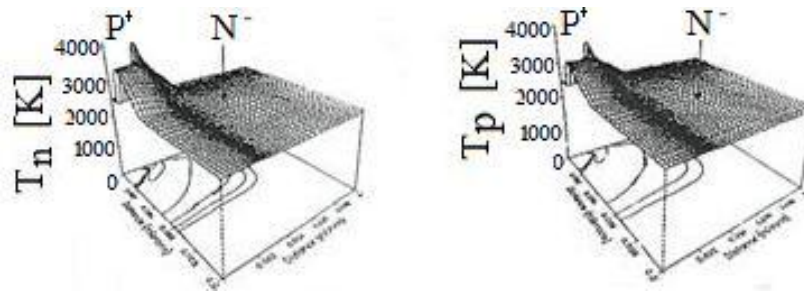


Figure 10. (a) Electron and (b) hole temperature distribution in the p-i-n diode (at -75V bias, 300K)

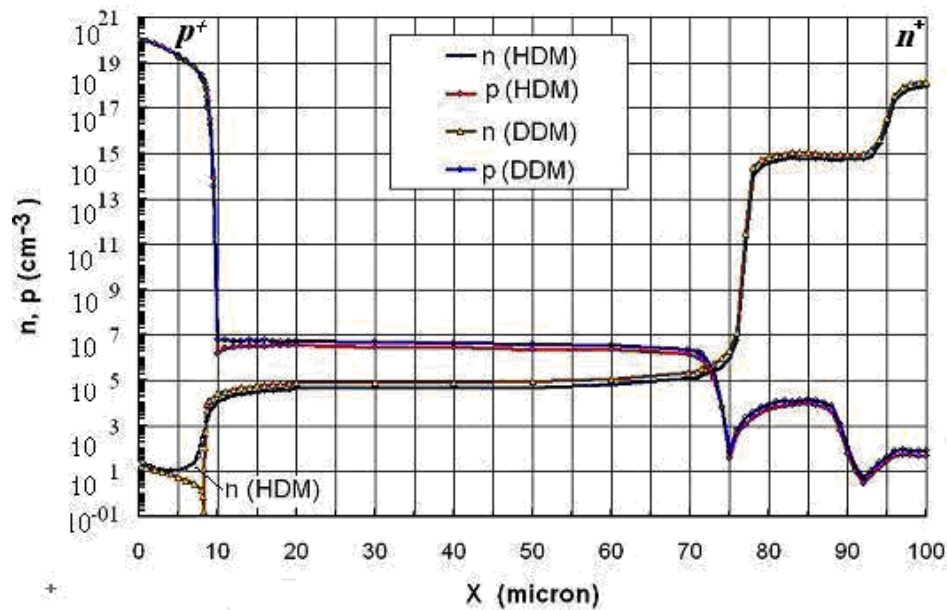


Figure 11. Electron density distribution along the p-i-n diode (at 500V reverse bias, 300K), on the basis of DDM and HDM

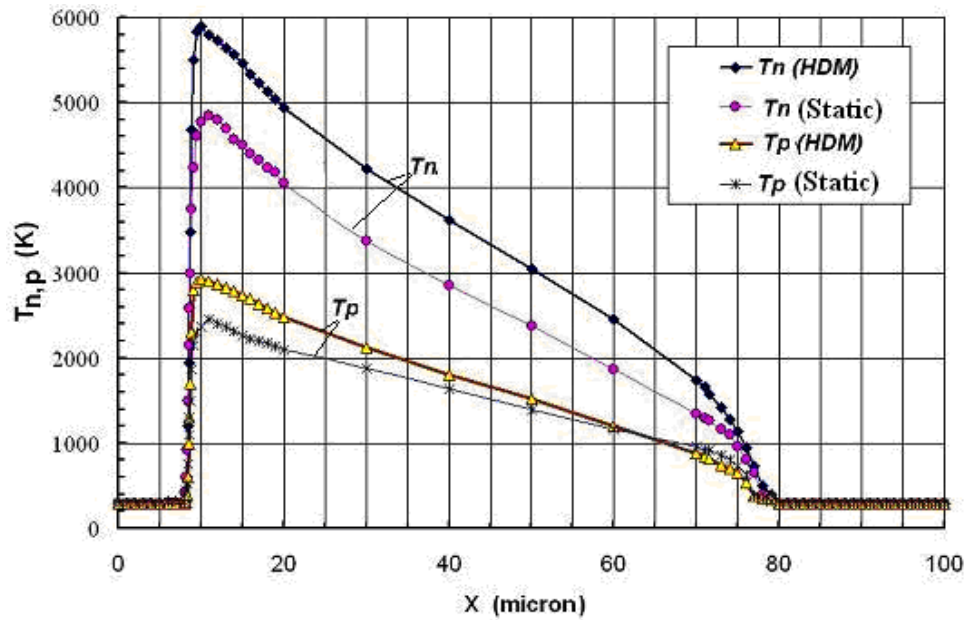


Figure 12. Electron and hole temperature distribution along a reverse biased p-i-n diode (at -500V), as calculated from the DDM electric field distribution (static) and by HD simulation

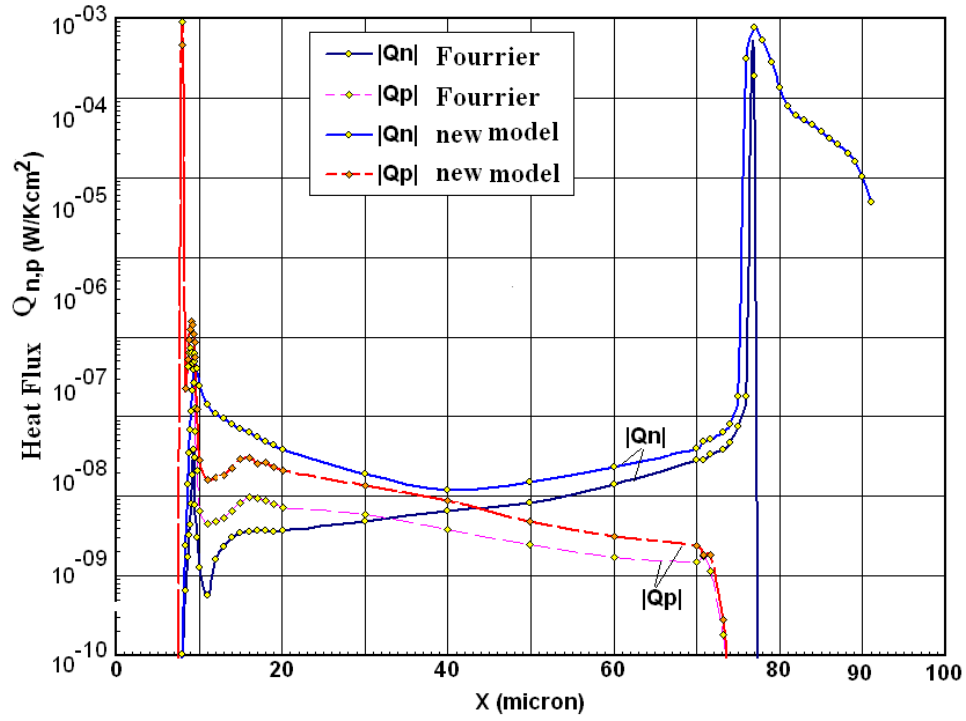


Figure 13. Electron heat flux distribution along the p-i-n diode at 500V reverse bias, 300K

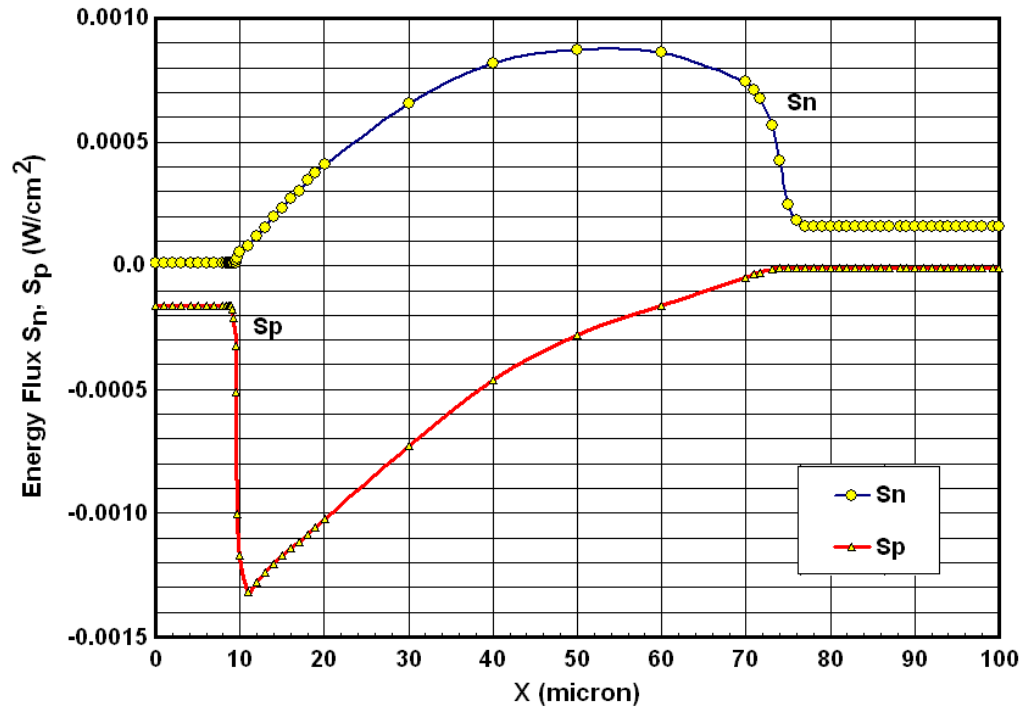


Figure 14. Electron energy flux distribution along the p-i-n diode at 500V reverse bias, 300K

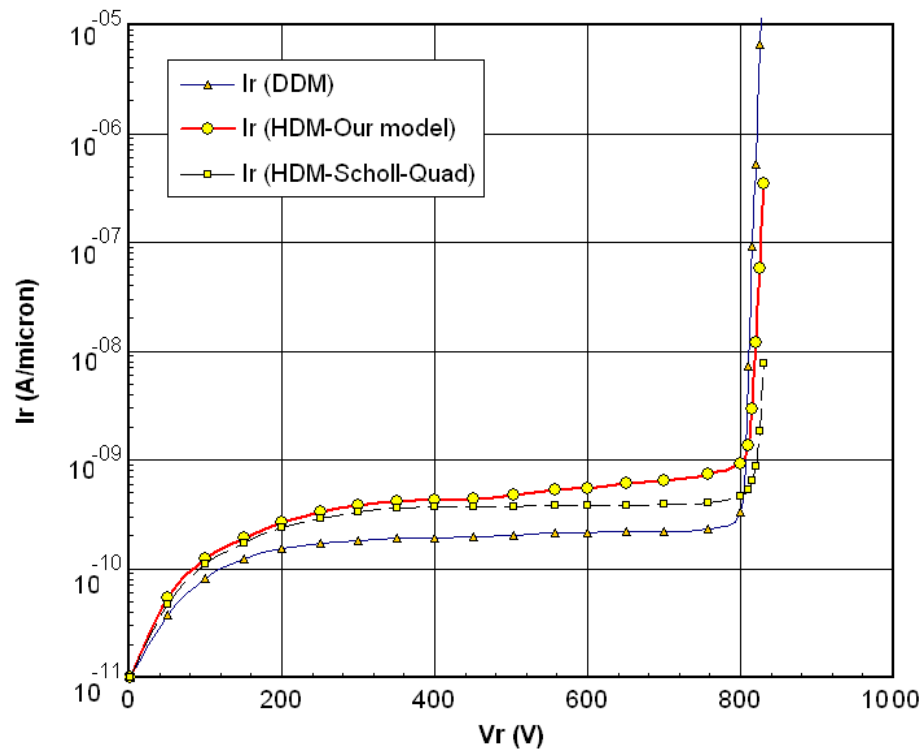


Figure 15. The I-V characteristics of the simulated the p-i-n diode near avalanche breakdown, as obtained by 2-dimensional DD and HD simulation at 300K. The surface of the p-i-n diode is properly passivated and protected by field plates, so that the breakdown occurs at the junction curvature inside the p-i-n diode

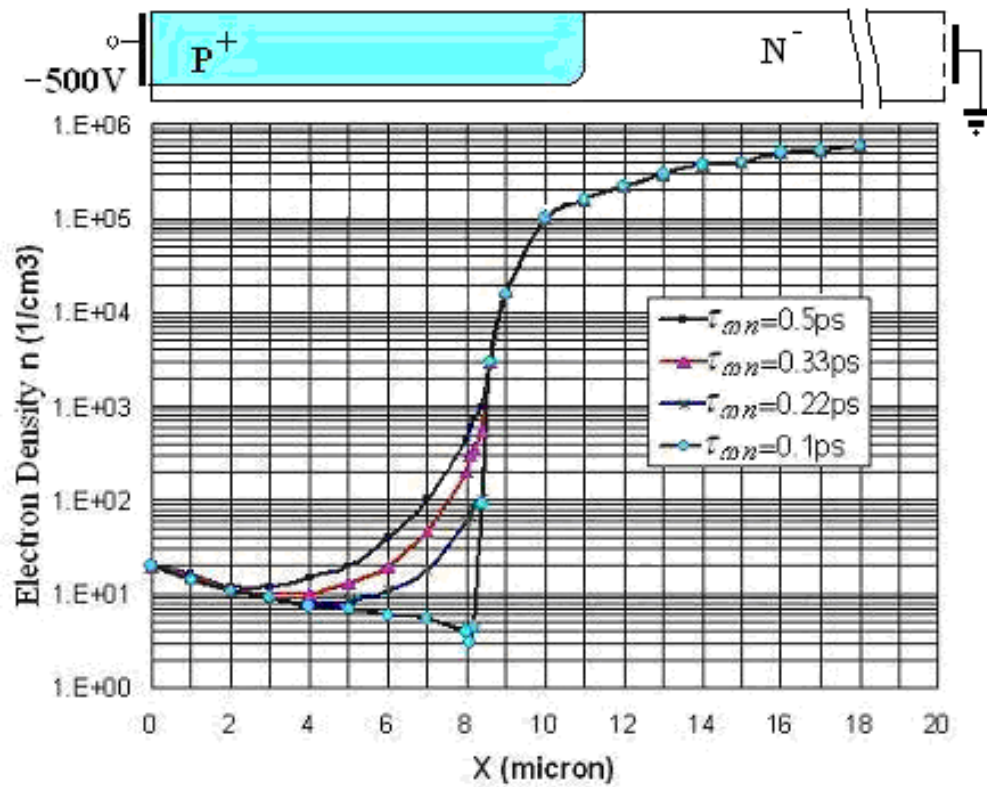


Figure 16. Electron density distribution along a reverse biased p-n junction, with different values of energy relaxation time

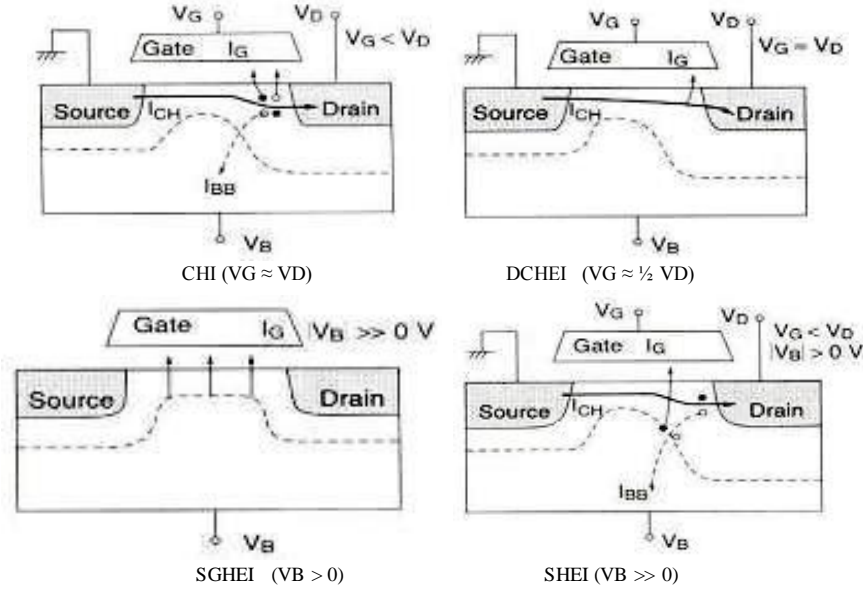


Figure 17. Illustration of different hot carrier injection mechanisms in MOSFET Devices

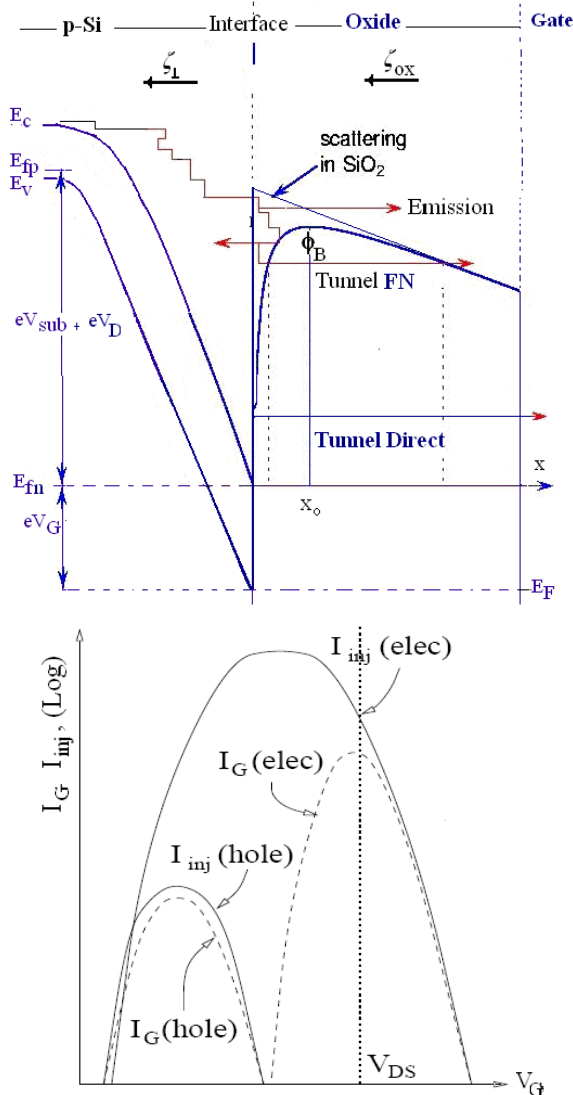


Figure 18. Illustration of hot carrier injection currents in MOSFET Devices

$$\omega_n = \omega_{n0} + e \cdot \tau_{wn} v_d \zeta \quad (54)$$

We may conclude from this discussion that the DDM simulation is a hypothetical case of the HDM where we assume $\tau_{on} = 0$ and hence $\omega_n = \omega_0$, and this case means a virtual semiconductor whose collisions are so efficient that electrons relax to their equilibrium energy in almost no time.

$$DDM = \lim_{\tau_{on} \rightarrow 0} HDM \quad (54)$$

The electrons in such a virtual semiconductor (with zero energy relaxation time) will not allowed to heat up even at high electric fields such that the mean electron energy ω_n will be almost equal to the lattice energy ω_{n0} . This result has been already reported for majority carriers in MOSFET devices[97], but has never been reported for minority carriers in bipolar devices, as far as the author knowledge.

10. Conclusions

In conjunction with sophisticated Monte Carlo methods that incorporate both realistic band structure and carrier scattering processes, the HDM is a basic tool to understand hot carrier behaviour in ever smaller and ultra fast semiconductor devices. We presented in this article a complete hydrodynamic model based on the first three moments of the semiclassical BTE for electrons, holes and phonons, with a few number of parameters. The model includes the band structure non-parabolicity effects and advanced energy-dependent models of the carrier mobility, impact ionization rate and heat flux. As the accurate estimation of the carrier temperature in semiconductor devices, influences the estimation of so many important parameters, such as the breakdown voltage and leakage currents, we proposed a simple definition of the carrier temperature, which takes the band structure into account. The definition results in temperatures which are closer to the Monte Carlo simulation results than those obtained by the

classical hydrodynamic models. We also proposed a phenomenological correlation between the electron average mass and energy relaxation time which cuts down the number of parameters of the HDM. In conclusion, our proposed system of HDE's has a few energy-dependent parameters (μ_n , α_n , m_n , τ_{en}) and they are all correlated to the energy relaxation time τ_{en} . The later parameter can be obtained from the MC simulation[161] or by measurement. The proposed model has been applied to investigate the

carrier transport in certain semiconductor devices and led to adequate results. From our simulation, we conclude that the undeliberated choice of the energy relaxation time value in the HD simulation leads to drastic results and may be to the failure of the HDM in certain cases, as reported in[47]. For instance, we show, by simulation, that reducing the energy relaxation time to unreasonable short values will mask the thermal diffusion mechanism and gives erroneous results, in both MOSFET and bipolar devices.

APPENDIX: Moments of the BTE

Consider the distribution function $f(x, k, t)$, which obeys the BTE. Consider $A(k)$ a microscopic quantity, which is a function of the wave vector k . Now, let's multiply the BTE by $A(k)$ and integrate the two sides of the equation over the entire k -space:

$$\int A \frac{\partial f}{\partial t} d^3k + \int A \mathbf{v}_g \cdot \nabla_x f d^3k + \int \frac{AF}{\hbar} \cdot \nabla_k f d^3k = \int A \left(\frac{\partial f}{\partial t} \right)_c d^3k \quad (55)$$

We have also, the mean value of $A(k)$, which we note by $\langle A \rangle$ is given by:

$$\langle A \rangle = \frac{\int A(k) f(k, r, t) d^3k}{\int f(k, r, t) d^3k} = \frac{\int A(k) f(k, r, t) d^3k}{n} \quad (56)$$

Therefore, the 1st term of the L.H.S of equation (55) becomes:

$$\int A \frac{\partial f}{\partial t} d^3k = \frac{\partial}{\partial t} \int A f d^3k = \frac{\partial (n \langle A \rangle)}{\partial t} \quad (57-a)$$

The 2nd term of the L.H.S of equation (55) becomes:

$$\int A \mathbf{v}_g \cdot \nabla_x f d^3k = \nabla_x \cdot \int A \mathbf{v}_g f d^3k - \int \nabla_x A \cdot \mathbf{v}_g f d^3k = \nabla_x \cdot (n \langle A \mathbf{v}_g \rangle) \quad (57-n)$$

Table 1. The integration of different terms of the LHS of the BTE, after being multiplied by $A(k)$

Moment	$A(k)$	$n \langle A \rangle$	$\langle (F \cdot \nabla_k) A / \hbar \rangle$	$\nabla_x \cdot (n \langle \mathbf{v}_g A \rangle)$
0	1	n	0	$\nabla_x \cdot (n \mathbf{v}_n)$
1	$\mathbf{u}_g(k)$	$n \langle \mathbf{v}_g \rangle = n \mathbf{v}_n$	$-\frac{1}{\hbar^2} \langle \nabla_k^2 E \rangle F = -\langle m^{*-1} \rangle F$	$\nabla_x \cdot (n \langle \mathbf{v}_g \otimes \mathbf{v}_g \rangle)$
2	$E_n(k)$	$n \langle E_n \rangle = n \omega_n$	$-n \mathbf{v}_n \cdot F$	$\nabla_x \cdot (n \langle E_n \mathbf{v}_g \rangle) = \nabla \cdot S_n$
3	$\mathbf{u}_g(k) E_n(k)$	$n \langle u_n E_n \rangle = S_n$	$-\langle m^{*-1} E_n + u_n \otimes u_n \rangle F$	$\nabla_x \cdot (n \langle E_n \mathbf{v}_g \otimes \mathbf{v}_g \rangle)$

Also, the 3rd term of the L.H.S of equation (55) becomes:

$$\int \frac{AF}{\hbar} \cdot \nabla_k f d^3k = \sum_j \left| \frac{f(k, x, t) A F_j}{\hbar} \right|_{-\infty}^{\infty} - \int f \nabla_k \cdot \left(\frac{AF}{\hbar} \right) d^3k \quad (57-d)$$

where we effectuated an integration by parts on the k -variable. The index j of the force component F_j appears for any orthonormal basis (e.g. for Cartesian coordinates, $j = x, y, z$). The totally integrated term in equation (I-2c) disappears because $\lim_{k \rightarrow \pm\infty} f(k, x, t) A(k) F_j = 0$. This means that all the moments of the BTE are finite. On the other hand, the second term of (I-2c) may be written as follows:

$$\langle \nabla_k \bullet \left(\frac{AF}{\hbar} \right) \rangle = \left\langle \left(\frac{F}{\hbar} \bullet \nabla_k \right) A \right\rangle + \langle \Delta \nabla_k \bullet \left(\frac{F}{\hbar} \right) \rangle = \left\langle \left(\frac{F}{\hbar} \bullet \nabla_k \right) A \right\rangle \quad (57)$$

Here, we put $\nabla_k \bullet F = 0$, which is true if F is independent of k or when F is normal to k . Fortunately, this is the case for electric field force ($F = -e\zeta$) and Lorentz's force ($F = -e\mathbf{v}_g \times B$). Now, by regrouping all (55) components we get:

$$\frac{\partial}{\partial t} n \langle A \rangle + n \left\langle \left(\frac{F}{\hbar} \bullet \nabla_k \right) A \right\rangle + \nabla_x \bullet (n \langle \mathbf{v}_g A \rangle) = \left[\frac{\partial}{\partial t} n \langle A \rangle \right]_c \quad (58)$$

By replacing $A(k)$ by 1 , $\mathbf{v}_g(k)$ and $E_n(k)$ we obtain the 3 moment equations of the BTE. Table 1 summarizes the results.

REFERENCES

-
- transport in Si," IEEE Trans. Electron. Dev., vol.41, no.9, pp. 1646-1654, 1994.
- [1] C. Cercignani, The Boltzmann equation and its applications, Springer-Verlag, 1988.
- [2] K. Hess, Advanced Theory of Semiconductor Devices, 352p., Wiley-IEEE Press, 1999.
- [3] N. Bogoliubov, Problemi dynami, Sov. Phys. JETP, vol. 10, p.256, 1946.
- [4] J. R. Barker, "Quantum transport theory of high-field conduction in semiconductors," J. of Physics C: Solid-State Physics, vol. 6, pp.2663-2684, 1973.
- [5] C. Buet., S. Dellacherie, R. Sentis, "Numerical solution of an ionic Fokker-Planck equation with electronic temperature", Society for Industrial and Applied Mathematics (SIAM), vol. 39, no.4, pp. 1219-1253, 2001.
- [6] A. Arnold, Quantum Fokker-Planck models: Kinetic versus density matrix formulations,[online]. Available: <http://mail.math.upstate.edu/~nanolab/Contents/Invited1.pdf>, 2004.
- [7] F. Capasso, Physics of Quantum Electron Devices, Heidelberg: Springer-Verlag, 1990.
- [8] P. Holland, The quantum theory of motion, Cambridge University Press, New York, 1993.
- [9] E. Wigner. On the quantum correction for thermodynamic equilibrium. Phys. Rev. vol. 40, pp. 749-759., 1932.
- [10] W. Frensley, "Wigner function model of a resonant tunneling semiconductor devices," Phys. Rev. B, vol. 36, no. 3, pp.1570-1580, 1987.
- [11] L. Shifren and D. Ferry, "Particle Monte Carlo simulation of Wigner function tunneling," Physics Letters A, vol. 285, pp.217-221, 2001.
- [12] T. Shawki, G. Salmer and O. El-Sayed, "2-D simulation of degenerate hot electron transport in MODFET's including DX center trapping" IEEE Trans. CAD, Vol 9, no. 1, pp.11-17, 1990.
- [13] M. Cramer and A. Crickenberger, "The Prandtl-Meyer function for dense gases," AIAA Journal, vol. 30, no. 4, pp. 561-564,1992.
- [14] A. Abramo et al., "A comparison of numerical solution of the Boltzmann transport equation for high-energy electron transport in Si," IEEE Trans. Electron. Dev., vol.41, no.9, pp. 1646-1654, 1994.
- [15] H.D. Rees, "Computer simulation of semiconductor devices," J. Phys. C:Solid-State Phys., vol. 6, pp. 266-273, 1973.
- [16] J-P. Aubert, J-C. Vassiere and J-P. Nougier, "Matrix determination of the stationary solution of the Boltzmann Equation for Hot Carriers in Semiconductors," J. Appl. Phys. vol. 56, no. 4, pp.1128-1132, 1984.
- [17] W. Fawcett, A. D. Boardman, and S. Swain, "Monte Carlo determination of electron transport properties in Gallium Arsenide," J. Physics and Chemistry of Solids, vol. 31, pp. 1963-1990, 1970.
- [18] C. Mogilestue, "Monte Carlo particle simulation of hot electron plasma formed in p-n junction," Electron. Lett., vol. 22, p. 397-379, 1972.
- [19] C. Jacoboni and P.Lugli, The Monte Carlo method for semiconductor device simulation, Springer-Verlag, Vienna, 1989.
- [20] K. Hess Ed., Monte Carlo device simulation: Full band and beyond, Kluwer Academic Press, Boston, 1991.
- [21] M. Fischetti, S. Laux, P. Solomon, and A. Kumar, "Thirty years of Monte Carlo simulations of electronic transport in semiconductors: Their relevance to science and mainstream VLSI technology", IBM Research Division, T. J. Watson Research Center, 10598 IWCE 10, Oct. 2004.
- [22] M. Saraniti and S. M. Goodnick, "Hybrid fullband cellular automaton/Monte Carlo approach for fast simulation of charge transport in semiconductors," IEEE Trans. Electron Devices, vol. 47, no. 10, 2000
- [23] T.-W. Tang and H. Gan, "Two formulations of semiconductor transport equations based on spherical harmonic expansion of the Boltzmann transport equation," IEEE Trans. Electron Devices, vol. 47, no. 9, 2000.
- [24] C. Jungemann, B. Meinerzhagen: "A Legendre Polynomial Solver for the Langevin Boltzmann Equation "J. Computational Electronics, vol. 3, pp. 157-160, 2004.
- [25] C. Jungemann, Matthias Bollhfer, B. Meinerzhagen" Convergence of the Legendre
- [26] Polynomial Expansion of the Boltzmann Equation for Nanoscale Devices " ESSDERC, pp. 341-344, Grenoble (France), 2005.
- [27] C. Auer and F. Schürer, "Efficient time integration of the Boltzmann-Poisson system applied to semiconductor device

- simulation," J. Computational Electronics, pp. 5-14, vol. 5, no.1, 2006.
- [28] S.F. Liotta and H. Struchtrup, "Moment equations for electrons in semiconductors: Comparison of spherical harmonics and full moments," Solid-State Electronics vol. 44, pp. 95-103, 2000.
- [29] R. Stratton, "Diffusion of hot and cold electrons in semiconductor barriers," Physical Review, vol. 126, pp. 2002-2014, 1962.
- [30] K. Bløtekjaer, "Transport equations for electrons in two-valley semiconductors," IEEE Trans. Electron devices, vol. ED-17, no. 1, pp. 38-47, 1970.
- [31] M.S. Shur and L.F. Eastman, "Near ballistic transport in GaAs devices at 77K," Solid-State Electronics, vol. 24, p. 11, 1981.
- [32] J-P. Nougier, J. Vassiere, D. Gasquet, J. Zimmermann and C. Constant, "Determination of the transient regime in semiconductor devices using relaxation time approximation," J. Applied Physics, vol. 52, pp.825-832, 1981.
- [33] R. Cook and J. Frey, "An efficient technique for 2-D simulation of velocity overshoot effects in Si and GaAs devices," COMPEL, vol. 1, pp. 65-87, 1982.
- [34] G. Baccarani G and M. Wordemann, "An investigation of steady-state velocity overshoot in Silicon", Solid-State Electronics, vol. 28, pp. 407-416, 1985.
- [35] C.C. McAndrew, E.L. Heasell and K. Singhal, "A comprehensive transport model for semiconductor device simulation," Semicond. Sci Technology, vol. 2, pp.643-648, 1987.
- [36] B. Meinerzhagen and W. Engl, "The influence of the thermal equilibrium approximation on the accuracy of classical 2-D numerical modeling of silicon submicrometer MOS transistors," IEEE Trans. Electron Devices, vol. ED-35, no.5, pp.689-97, 1988.
- [37] N. Goldsman and J. Frey, "Efficient use of the energy transport method in device simulation," IEEE Trans. Electron Devices, vol. 35, no. 9, 1988.
- [38] M. Cheng and Kunhardt, "A theory of non-equilibrium carrier transport in multivalley semiconductors," J. Applied Physics, vol. 67, no. 4, pp. 1907-1914, 1990.
- [39] M. R. Thoma et al., "Hydrodynamic equations for semiconductors with nonparabolic band structures," IEEE Trans. on Electron Devices, vol. 38, no. 6, pp.1343-1352, 1991.
- [40] D. Chen, E.C. Kan, U. Ravaioli, W.-C Shu and R.W. Dutton, "An improved energy transport model including nonparaboility and non-Maxwellian distribution Effects," IEEE Trans. Electron Dev. Lett., vol. 13, no. 1, pp.26-28, 1992.
- [41] T-W. Tang and J. Nam, "An improved hydrodynamic transport model for silicon," IEEE Trans. Electron Devices, vol. 40, no. 8, 1993.
- [42] C.-S. Yao et al., "Formulation of a tail electron hydrodynamic model based on Monte Carlo results," Electron Dev. Lett., vol. 16, no. 1, pp. 26-29, 1995.
- [43] M. Jeong and T-W. Tang, "Influence of hydrodynamic models on the prediction of submicrometer device characteristics," IEEE Trans. on Electron Devices, vol. ED-44, no. 12, 1997.
- [44] A. M. Anile, V. Romano and G. Russo, "Extended hydrodynamic model of carrier transport in semiconductors," SIAM J. Applied Math, vol. 61, no. 1, pp. 74-101, 2000.
- [45] T. Grasser, H. Kossina, M. Gritsch and S. Selberherr, "Using six moments of Boltzmann's transport equation for device simulation," J. Appl. Phys., vol. 90, no. 5, pp.2389-2396, 2001.
- [46] M. Gritsch, H. Kosina, T. Grasser, and S. Selberherr, "Revision of the standard hydrodynamic transport model for SOI simulation," IEEE Trans. Electron Devices, vol. ED-49, no. 10, pp.1814-1820, 2002.
- [47] T. Grasser, T-W. Tang, H. Kosina and S. Selberherr, "A review of hydrodynamic and energy-transport models for semiconductor device simulation," Proceedings of IEEE, vol. 91, no. 2, pp.251-274, 2003.
- [48] C.Jungemann, T. Grasser, B.Neinhilus and B.Meinerzhagen, "Failure of moment-based transport models in nanoscale devices near equilibrium," IEEE Trans. Electron Dev., vol. 52, no. 11, pp. 2404-2408, 2005.
- [49] G.K. Batchelor, An Introduction to Fluid Dynamics, Cambridge Univ. Press, New York, 1967.
- [50] I. Muller and T. Ruggeri, Extended Thermodynamics, Springer-Verlag, Berlin, 1993.
- [51] S. M. Sze, Physics of Semiconductor Devices, Wiley, New York, 1986.
- [52] J. Fourier, Théorie Analytique de la Chaleur, 1822, Reprint ISBN 2-87647-046-2, 670p, Gabay, 1988.
- [53] H. Fröhlich, "On the theory of dielectric breakdown in solids," Proc. Royal Soc., London, vol. 188-A, pp.521-532, 1947.
- [54] J. Higman and K. Hess, "Comment on the use of the electron temperature concept for nonlinear transport problems in semiconductor p-n junctions," Solid-State Electronics, vol. 29, no. 9, pp 915-918, 1986.
- [55] W. Engl and H.K. Dorks, Models of physical parameters, in: An introduction to numerical analysis of semiconductor devices and integrated circuits, Boole Press, Dublin, 1981.
- [56] S. Selberherr, On Modeling MOS-Devices, in: Simulation of semiconductor devices, Chapter 8, Elsevier Science Publishers, North-Holland, 1986.
- [57] D. Caughey and R. Thomas, "Carrier mobility in silicon empirically related to doping and field," IEEE Proceedings, vol. 54, pp. 2192-2193, 1967.
- [58] J.M. Dorkel and Ph. Leturcq, "Carrier mobilities in silicon semi-empirically related to temperature, doping and injection level, Solid-State Electronics, vol. 24, pp. 821-825, 1981.
- [59] D. B. Klassen, "A unified mobility model for device simulation-Part I: Model equations and concentration dependence," Solid-State Electron., vol. 35, no. 7, pp.953-959, 1992.
- [60] C. Canali, G. Majni, R. Minder and G. Ottaviani, "Electron and hole drift velocity measurements in silicon and their

- empirical relation to electric field and temperature," IEEE Trans. Electron Devices, vol. ED-22, pp. 1045-1047, 1975.
- [61] M. H. El-Saba, "Accurate modeling of hot-carrier drift mobility in semiconductor devices," Proceedings of the Int. Conf. of Microelectronics ICM VI, Cairo, 1995.
- [62] W. Hänsch and M. Miura-Mattausch, "The hot-electron problem in small semiconductor devices," J. Appl. Phys. vol. 60, pp. 650-656, 1986.
- [63] M. H. El-Saba, Modélisation hydrodynamique des phénomènes de transport des porteurs chauds et de l'ionisation par impact dans les dispositifs à semiconducteur, PhD Thesis, INSA Lyon, France, Order no. 93 ISAL 0072, 1993.
- [64] K.K. Thornber, "Relation of drift velocity to low-field mobility and high-field saturation velocity," J. Appl. Phys., vol. 51, pp. 2127-2136, 1980.
- [65] A. G. Sabins and J.T. Clemens, "Characterization of the electron mobility in the inverted (100) Si surface," IEDM Tech. Digest, Dec. 1979, pp. 18-21.
- [66] K. Yamaguchi, "A mobility model for carriers in the MOS inversion layer," IEEE Trans. Electron Devices, vol. 30, pp. 658-663, 1983.
- [67] S.A. Schwarz et al., "Semi-empirical equations for electron velocity in silicon: Part II- MOS inversion layer," IEEE Trans. Electron Devices, vol. ED-30, no. 12, pp.1634-1639, 1983.
- [68] M. Liang, J. Choi, P.K. Ko and C. Hu, "Inversion-layer capacitance and mobility of very thin gate oxide MOSFETs," IEEE Trans. Electron Devices, vol. 33, p. 409, 1986
- [69] J. E. Chung, P.K. Ko and C. Hu, "A model for hot-electron - induced MOSFET linear-current degradation based on mobility reduction due to interface-state generation," IEEE Trans. Electron Devices, vol. 38, no. 6, pp. 1362-1370, 1991.
- [70] S. Takagi, A. Toriumi, M. Iwase and H. Tango, "On the universality of inversion layer mobility in Si. MOSFETs – Part I: Effects of substrate impurity concentration," IEEE Trans. Electron Devices, vol. 41, no. 12, pp. 2357-2362, 1994.
- [71] M. N. Darwish, J. L. Lentz, M. Pinto, P. Zeitoff, T. J. Krutsick and H. Ha Vuong, "An Improved electron and hole mobility model for general purpose device simulation," IEEE Trans. Electron Devices, vol. 44, no. 9, pp. 1529-15338, 1997.
- [72] C. Lombardi, S. Manzini, A. Saporito and M. Vanzi, "A physically-based mobility model for numerical simulation of nonpolar devices," IEEE Trans. Computer-Aided Design, vol. 7, no. 11, pp. 1164-1171, 1988.
- [73] K. G. McKay, "Avalanche breakdown in Si," Phys. Rev. vol. 94, pp.877-884, 1954.
- [74] P. A. Wolff, "Theory of multiplication in silicon and germanium," Phys. Rev., vol. 95, no. 6, pp.1415-1420, 1954.
- [75] G.A. Baraff, "Distribution function and ionization rates for hot electrons in semiconductors, Phys. Rev. , vol. 128, no. 6, pp. 2507-2517, 1962.
- [76] L. V. Keldish, "Concerning the theory of impact ionization in semiconductors," Sov. Phys. JETP, vol. 21, pp. 1135-1144, 1965.
- [77] A. G. Chynoweth, "Ionization rates for electrons and holes in Si," Phys. Rev. vol. 109, no. 5, pp.1537-1540, 1958.
- [78] C. A. Lee, R.A. Logan, R.L. Latdorf, J. Klimack and W. Wiegmann, "Ionization rates of holes and electrons in Si p-n junctions," Phys. Rev. A, vol. 134, pp.761-773, 1964.
- [79] R. Van Overstatten and H. De Man, "Measurement of the ionization rates in diffused Si p-n junctions," Solid-State Electronics, vol. 13, pp.583-608, 1970.
- [80] N. Kotani and S. Kawazu, "A Numerical analysis of avalanche breakdown in short-channel MOSFETs," Solid - State Electronics, vol. 24, pp. 681-687, 1981.
- [81] W. Maes, K. de Meyer, and R. Van Overstraeten, "Impact ionization in silicon: A review and update," Solid-State Electron., vol. 33, pp.705–718, 1990.
- [82] I. Takayanagi, K. Matsumoto, and J. Nakamura, "Measurement of electron impact ionization coefficient in bulk silicon under a low-electric field," J. Appl. Phys., vol.72, pp.1989–1992, 1992.
- [83] W. Grant, "Electron and hole ionization rates in epitaxial silicon at high electric fields," vol. 16, pp. 1189-1203, 1973.
- [84] W. Shockley, "Problems related to p-n junctions in silicon," Solid-state Electronics, vol. 2, pp.35-67, 1961.
- [85] S. Tam et al., Hot-electron current in very short channel MOSFETs," IEEE Trans. Electron Dev. Lett., vol. 4, pp.249 - 251, 1983.
- [86] Y-Z. Chen and T-W. Tang, "Numerical simulation of avalanche hot-carrier injection in short-channel MOSFETs," IEEE Trans. Electron Devices, vol. 35, no. 12, 1988.
- [87] N. Goldsman, L. Henrickson and J. Frey, "Reconciliation of a hot-electron distribution function with lucky electron exponential model in silicon," IEEE Electron Dev. Let., vol. 11, no. 10, 1990.
- [88] E. Schöll and W. Quade, "Effect of impact ionization on hot-carrier energy and momentum relaxation in Semiconductors", J. Physics C. Solid-State Phys., vol. 20, pp. L861-L867, 1987.
- [89] W. Quade, E. Schöll, and M. Rudan, "Impact ionization within the hydrodynamic approach to semiconductor transport," Solid-State Electronics, vol. 36, no. 10, pp.1493 – 1505, 1993.
- [90] K. Souissi, F. Odeh, H. Tang, A. Gnudi and P-F. Lu, "Investigation of the impact ionization in the hydrodynamic model," IEEE Trans. Electron Dev. vol. 40, no. 8, pp. 1501 - 1507, 1993.
- [91] E. Crabbe, J. Stork, G. Baccarani, M. Fischetti and S. Laux, "The impact of non-equilibrium transport on Breakdown in Transit Time in Bipolar Transistors," IEDM Tech. Dig, p.463, 1990.
- [92] D. Cassi and B. Ricco, "An analytical model of the energy distribution of hot electrons," IEEE Trans. Electron Devices, vol. 37, no. 6, pp. 1514-1521, 1990.
- [93] K. Matsuzawa, I. Kamohara and T. Wada, "Device simulation including energy transport with improved Physical Models," NASECODE VII Trans., J.J. Miller Ed., Colorado, pp.173 - 174, 1991.

- [94] C.-S. Yao et al., "Formulation of a tail electron hydrodynamic model based on Monte Carlo results," *Elec. Dev. Lett.*, vol. 16, no. 1, pp. 26-29, 1995.
- [95] H.J. Peifer, B. Meinerzhagen, R. Thoma and W.L. Engl, "Evaluation of impact ionization modeling in the framework of hydrodynamic equations," *IEDM Tech. Digest*, 1991.
- [96] T. Grasser, H. Kosina and S. Selberherr, "Influence of the distribution function shape and band Structure, on impact ionization modelling," *J. Appl. Phys.* vol. 90, no. 12, pp. 6165-6171, 2001.
- [97] K. Sonoda, S. T. Dunham, M. Yamaji, K. Taniguchi and C. Hamaguchi, "Impact ionization model using average energy and average square energy distribution," *Japan. J. Appl. Phys.*, vol. 35, no. 2B, pp. 818-825, 1996.
- [98] T. Grasser, H. Kosina, C. Heitzinger and S. Selberherr, "An impact ionization model including an explicit cold carrier population," *Modelling and Simulation of Microsystems*, ISBN 0-9708275-7-1, 2002.
- [99] H. C. Morris, M. M De Pass and Henok Abebe, "Analytic formulae for the impact ionization rate for use in compact models of ultra-short semiconductor devices," *Proceedings Nanotechnology Conference*, vol. 2, pp.140-143, Boston, Massachusetts, USA, 2004.
- [100] P. G. Scrobhaci and T.-W. Tang, "Modeling of the hot electron subpopulation and its application to impact ionization in submicron silicon devices- PART I: Transport equations," *IEEE Trans. Electron Devices*, vol. 41, no.7, p.1197, 1994.
- [101] C.S. Yao, J.G. Ahn, Y.-J. Park, H.-S. Min and R.W. Dutton, "Formulation of a tail electron hydrodynamic model based on Monte Carlo results," *IEEE Electron Devices Lett.*, vol. 16, no. 1, p. 26, 1995.
- [102] T.-W. Tang and J. Nam, "A simplified impact ionization model on the average energy of hot-electron subpopulation," *IEEE Electron Devices Lett.*, vol. 19, no. 6, 1998.
- [103] M. H. El-Saba, "Accurate hydrodynamic modeling of impact ionization rate in semiconductor devices," *Int. Conf. on Radio Science, URSI*, Cairo, 1998.
- [104] K. K. Thornber, "Application of scaling to problems in high-field electronic transport," *J. Appl. Phys.*, vol. 52, no. 1, pp. 279-290, 1981.
- [105] J. Bude and K. Hess, "Threshold of impact ionization in semiconductors," *J. Appl. Phys.* vol. 72, no. 8, 1992.
- [106] J. Tang, "Theoretical studies of high field transport in GaAs, Si and heterostructures," *PhD Dissertation*, Univ. of Illinois, Urbana, 1983.
- [107] C. Crowell and S. M. Sze, "Temperature dependence of avalanche multiplication in semiconductors," *Appl. Phys. Lett.*, vol. 9, no. 6, p. 242, 1966..
- [108] R. A. Ballinger, K.G. Major and J.R. Mallinson, "Impact ionization thresholds in semiconductors," *J. Phys. C: Solid-state Phys.*, vol. 6, pp. 2573-2585, 1973.
- [109] Ken Kai-fu Chang, Kajen R. S., Shen Chen, Ping Bai, Ganesh Samudra and Erping Li, "Investigation on the Impact Ionization Breakdown Onset of Double-Gate MOSFET structure with Optimized Hydrodynamic Model via Full-band Monte Carlo Method," *IEEE Trans. Vol. 46, No. 2*, pp. 221-231, 2008.
- [110] K. Hess, "Comment on effect of collisional broadening on Monte Carlo simulation of high-field transport in semiconductor devices," *IEEE Electron Devices Lett.*, Vol EDL-2, pp.297-298, 1989.
- [111] F. R. McFeely, E. Cartier and E. Eklund, "New zero-field probes for the transport dynamics of very hot electrons," *Proceedings of NASECODE VIII*, J.J. Miller (Ed.), Vienna, Austria, pp.42-43, 1992.
- [112] W. Quade and Eckehard Scholl, F. Rossi, C. Jacoboni, "Quantum theory of impact ionization in coherent high-field semiconductor transport," *The American Physical Society*, April 1994
- [113] G. Wolodkin and J. Frey, "Overshoot effects in the relaxation time approximation," *Proceedings NASCODE 8*, Vienna, 1992, pp. 107-108.
- [114] C. Jacoboni and L. Reggiani, "Bulk hot-electron properties of cubic semiconductors," *Advanced in Physics*, vol. 28, pp. 493-553, 1983.
- [115] K. Seeger, *Semiconductor Physics*, Springer Verlag, 1973.
- [116] M. Costato and L. Reggiani, "Electron energy relaxation time in Si and Ge," *J. Phys. Chem. Solide*, vol. 34, pp.547-564, 1973.
- [117] B. Gonzalez et al., "An analytical Energy relaxation time model for device simulation," *Solid-State Electron.*, vol. 43, 1999.
- [118] D. Munteanu, G. Le Carval and G. Guegan, "Impact of non-stationary transport effects on realistic 50nm MOS technology," *Modelling and Simulation of Microsystems*, 2001.
- [119] K. Suzuki, K. Saito, K. Muraki and Y. Hirayama, "Photoluminescence from a modulation-doped Al_{0.33}Ga_{0.67}As/GaAs heterointerface under cyclotron resonance" *Phys. Rev.*, vol. B58, p.15385, 1998.
- [120] D. M. Rife, *J. Optical Soc. America*, vol. B 19, p.1092, 2002.
- [121] A. J. Sabbah and D. M. Riffe, "Femtosecond pump-probe reflectivity study of silicon carrier dynamics," *Phys. Rev. B*, vol. 66, pp. 165217-165228, 2002.
- [122] A. Matulionis, J. Liberis, L. Eastman, W. Schaff, J. Shealy, X. Chen and Y.-J. Sun, "Electron transport and microwave Noise in MBE-and MOCVD-Grown AlGaIn/AlN/GaN," *Acta Physica Polonica A*, vol. 107, pp. 361-364, 2005.
- [123] I. Bork, C. Jungemann, B. Meinerzhagen, W. L. Engl, "Influence of heat flux on the accuracy of hydrodynamic models for ultrashort Si MOSFETs," in *NUPAD Tech. Dig.*, Honolulu, 1994.
- [124] M. Ieong and T.-W. Tang, "Influence of hydrodynamic models on the prediction of submicrometer device characteristics," *IEEE Trans. Electron Devices*, vol. ED-44, no. 12, 1997.
- [125] M. H. El-Saba, "Problems related to the hydrodynamic model", *Proceedings of the 5th Int. Conference on Microelectronics ICM VI*, Cairo, 1995.
- [126] K. Hasnat, C-F. Yeap, S. Jallepalli, S. A. Hareland, W.K. Shih, V.M. Agostinelli, A.F. tasch and C. M. Maziar,

- "Thermoionic emission model of electron gate current in submicron NMOSFETs," *IEEE Trans. Electron Devices*, vol. 44, no. 1, pp. 129-138, 1997.
- [127] A. Gehring, T. Grasser, and S. Selberherr, "Non-parabolicity and non-Maxwellian effects on gate oxide tunneling," *The NSTI Nanotech. Conf. Proceedings*, Boston, 2003.
- [128] M. Rasras, I. De Wolf, G. Groeseneken, Ben Kaczer, R. Degraeve and H.E. Maes, "Photo-carrier generation as the origin of Fowler-Nordheim-induced substrate hole current in thin oxides," *IEEE Trans. Electron Devices*, vol. 48, no. 2, pp. 231-238, 2001.
- [129] T. H. Ning, C. M. Osburn, and H. N. Yu, "Emission probability of hot electrons from silicon into silicon dioxide," *J. Appl. Phys.*, vol. 48, pp. 286-293, 1977.
- [130] C. Hu, S. Tam, F. Hsu, P. Ko, T. Chan, and K. Terill, "Hot-electron-induced Mosfet degradation-Model, monitor and improvement," *IEEE Trans. Electron Devices*, vol. 32, no.2, p. 375-384, 1985.
- [131] J. D. Bude, "Gate current by impact ionization feedback in sub-micron MOSFET technologies," in *Proc. Symp. VLSI Tech.*, 1995, pp. 101-102.
- [132] D. R. Nair, S. Shukuri and S. Mahapatra, "Cycling endurance of NOR flash EEPROM cells under CHISEL programming operation—Impact of technology parameters and scaling," *IEEE Trans. Electron devices*, vol. 51, no. 10, pp. 1672-1678, 2004.
- [133] J. Egle, B. Polsky, B. Min, E. Lyumkis, O. Penzin, and M. Foisy, "SOI related simulation challenges with moment-based BTE solvers," *Simulation of Semiconductor Processes and Devices*, Seattle, Washington, USA, pp. 241-244, Sept. 2000.
- [134] M. Gritsch, H. Kosina, T. Grasser, S. Selberherr, T. Linton, S. Singh, S. Yu, and M.D. Giles, "The failure of the hydrodynamic transport model for simulation of partially depleted SOI MOSFETs and its revision," in *SIO Technology and Devices X*, (Washington DC, USA), pp. 181-186, 2001.
- [135] E. Pop, K. Banerjee, Per Sverdrup, R. Dutton and K. Goodson, "Localized heating effects and scaling of Sub-0.18 micron CMOS devices," *Int. Electron Devices Meeting (IEDM)*, 2002.
- [136] M. Cardona, *Fundamentals of Semiconductors*, Springer - Verlag, Berlin, 1996.
- [137] M-Y Chuang and M. E. Law, "A new algorithm for faster full-thermodynamic device simulations," *IEEE Trans. Electron Devices*, vol. 44, no. 9, 1997.
- [138] C. Kittel, *Introduction to Solid-State Physics*, New York, Wiley & Sons, 1967.
- [139] A. Chrysafis and W.A. Love, "Computer-aided analysis of one-dimensional thermal transients in n-p-n Power transistors," *Solid-state Electron.* vol. 22, pp. 249-256, 1979.
- [140] J. C. Glassbender and G.A. Slack, "Thermal conductivity of silicon and germanium from 3K to the melting point," *Phys. Rev. A*, vol. 134, pp. 1058-1069, 1964.
- [141] P. Su, K-I. Goto, T. Sugii, and C. Hu, "A thermal activation view of low voltage impact ionization in MOSFETs," *IEEE Electron Devices letters*, vol. 23, no. 9, pp.550- 552, 2002.
- [142] M. Asheghi, Touzelbaev, M.N., K.E. Goodson, Y.K. Leung and S.S. Wong, "Temperature-dependent thermal conductivity of single-crystal silicon layers in SOI substrates," *ASME Journal of Heat Transfer*, vol. 120, pp. 31-36, 1998.
- [143] P. G. Sverdrup, O. Tornblad, K. Banerjee, D. Yergeau, Z. Yu, R. W. Dutton and K. E. Goodson, "Advanced electro-thermal modeling and simulation Techniques for deep Submicron devices," *Techcon*, 2000.
- [144] D. A. Romanov, B. A. Glavin, and V. V. Mitin, "Stimulated decay of non-selectively pumped optical phonons in GaAs," *Phys. Rev. B* vol. 60, no. 7, 1999.
- [145] C. Gardner, "The quantum hydrodynamic model for semiconductor devices," *SIAM Journal on Applied Mathematics*, vol. 54, pp. 409-427, 1994.
- [146] D. Ferry, H. Grubin, "Modelling of quantum transport in semiconductor devices," *Solid State Phys.* 49 , pp.283-448, 1995.
- [147] I. Burghardt, S. Lorenz, S. Cederbaum, K. B. Moller, G. Parlant, "Hydrodynamic methods for ultrafast quantum dynamics, quantum transport, and dissipation," [online]. Available: <http://mail.math.ups-tlse.fr/~nanolab/Contents/Invited2.pdf>, 2004.
- [148] E. Madelung, "Quantentheorie in hydrodynamischer form," *Z. Physik*, vol. 40, pp.322-326, 1927.
- [149] Ansgar Jungel and D. Matthes, "A derivation of the isothermal quantum hydrodynamic equations using entropy minimization," *Appl. Numer. Math.*, 2005.
- [150] D. Ferry and J.-R. Zhou, "Form of the quantum potential for use in hydrodynamic equations for semiconductor device modeling," *Phys. Rev. B*, vol. 48, pp. 7944-7950, 1993.
- [151] C. Gardner and C. Ringhofer, "The smooth quantum potential for the hydrodynamic Model," *Phys. Rev.* vol. E53, pp.157 - 167, 1996.
- [152] C.S. Rafferty et al., "Multi-dimensional quantum effect simulation using a density-gradient model and script-level programming techniques," *SISPAD'98*, Leuven, Belgium, Sept., 1998, p.137.
- [153] D. Connelly, Z. Yu and D. Yergeau, "Macroscopic simulation of quantum mechanical effects in 2-D MOS devices via the density gradient method," *IEEE Trans.* vol. 49, no. 4, pp. 619-626, 2002.
- [154] H.U. Baranger and J.W. Wilkins, "Ballistic structure in the electron distribution function of small semiconducting structures: General features and specific trends," *Phys. Rev. B*, vol. 36, pp.1487-1502, 1987.
- [155] M.S. Lundstrom, "Elementary scattering theory of the MOSFET," *IEEE Electron Dev. Lett.*, vol. 18, pp.361-363, 1997.
- [156] M. Lundstrom and Zhibin Ren, "Essential physics of carrier transport in nanoscale MOSFETs," *IEEE Trans. Electron Devices*, vol. 49, no. 1, 2002.
- [157] K. Banoo, J.-H. Rhew, M. Lundstrom, C.-W. Shu and J. W. Jerome, "Simulating quasi-ballistic transport in Si nanotransistors," *7th Int. Workshop Computational Electronics, IWCE*, July, 2000.

- [158] W. C. Leonard, F. Register and S.K. Banerjee, Simulation of quantum effects along the channel of ultrathin Si-based MOSFETs," IEEE Trans. vol. 49, no. 4, pp. 652-657, 2002
- [159] A. Svizhenko and M.P. Arantvan, "Role of scattering in nanotransistors," IEEE Trans. Vol. 50, no. 6, pp. 1459-1466, 2003.
- [160] M. H. El-Saba, "Investigation of the hot carriers rebelling effect in semiconductor devices, Using an Analytical Solution of the Hydrodynamic Model," IEEE Trans. Electron Devices, vol. 52, no. 7, pp. 1561-1568, 2006.
- [161] Shiyu Chen, Kunyuan Xu, and Gang Wang , "Monte Carlo Investigation of Size-Dependent Impact Ionization Properties in InP Under Submicron Scale, Journal of Lightwave Technology, Vol. 27, Issue 10, pp. 1347-1354, 2009.